

LEIDEN UNIVERSITY

MASTERS THESIS

Opto-Mechanical Design for a Single Laser Adaptive Optics System for METIS

Author:

Alex Tripsas

Supervisor:

Dr. Remko Stuik &
Prof. Bernhard Brandl

*A thesis submitted in fulfillment of the requirements
for the degree of Masters Thesis 1*

in the

METIS Group
Astronomy and Instrumentation

August 1, 2019

Declaration of Authorship

I, Alex Tripsas, declare that this thesis titled, "Opto-Mechanical Design for a Single Laser Adaptive Optics System for METIS" and the work presented in it are my own. I confirm that:

- This work was done wholly or mainly while in candidature for a research degree at this University.
- Where any part of this thesis has previously been submitted for a degree or any other qualification at this University or any other institution, this has been clearly stated.
- Where I have consulted the published work of others, this is always clearly attributed.
- Where I have quoted from the work of others, the source is always given. With the exception of such quotations, this thesis is entirely my own work.
- I have acknowledged all main sources of help.
- Where the thesis is based on work done by myself jointly with others, I have made clear exactly what was done by others and what I have contributed myself.

Signed:



Date: 31 July 2019

*"Now is the moment that everything can change
You are completely responsible for your own life
And no one is coming to save you from yourself
So stop blaming your problems on any or everything else
It does not matter one tiny [obscenity] bit
How unfair you think the world is
It's only what you do
Right here, right now
Right this [obscenity] instant that matters
It's your choice to
Sink or swim"*

D. Randall Blythe

LEIDEN UNIVERSITY

Abstract

Astronomy Department
Astronomy and Instrumentation

Masters Thesis 1

Opto-Mechanical Design for a Single Laser Adaptive Optics System for METIS

by Alex Tripsas

The first generation of instruments on the upcoming ELT all need to use adaptive optics to take advantage of the 39 meter aperture the ELT offers. This is due to the fact that as the telescope diameter gets larger than the Fried parameter, more aberrations and speckles appear in the image. There are several ways to implement an AO system. Initially Laser Tomography AO was looked into for its uniform correction and wider FoV. However, due to its high cost and complexity, other options needed to be looked into. Previous research has shown that Single Laser AO could still provide sufficient wavefront correction for METIS. This thesis covers the process to design a cheaper alternative to the LTAO system planned for METIS. The designed optical layout has all spherical surfaces except for one aspherical surface, a telescoping mirror system for altitude correction, glass all made of the same material, and is compact ($1.2m \times 900mm \times 400mm$). The static optical system has a WFE of 0.0893 waves (52.6nm) RMS and 0.397 waves (233 nm) PTV .

Acknowledgements

I'd like to thank Dr. Remko Stuik for putting up with me twice a week and really driving me to fully understand what I was doing and teaching me many valuable skills.

Benjamin Arcier for all the work he did up until his graduation and continuing to be a great person to talk to afterwards.

To all my old colleagues back at University of California Santa Cruz for, despite me not being there anymore, to continue to help me. Notably, Will Deich and Rion Parsons, if it weren't for you, this research would have been a nightmare.

My long time friend Patrick Hoge, who helped me put together images that were outside of my Photoshop abilities. He will be cited where applicable

Lastly, Professor Bernhard Brandl for communicating with me even before I was officially a student and believing that I could bring something to this project with METIS.

Contents

Declaration of Authorship	iii
Abstract	vii
Acknowledgements	ix
1 Introduction	1
1.1 History of Adaptive Optics	2
1.2 Single Conjugate Adaptive Optics	4
1.3 Single Laser Adaptive Optics	5
1.4 Laser Tomography Adaptive Optics	7
1.5 METIS Science Goals	8
1.6 Focus of the Thesis	9
2 Mechanical Design of Initial Optical Design	11
2.1 Mechanical Constraints	11
2.2 Mechanical Components	12
3 Optical Design	15
3.1 Optical Constraints	15
3.1.1 Lenslet Array Calculations	16
3.1.2 Design of First Lens	17
3.1.3 The Rest of the System	18
3.2 Mirror Systems	19
3.3 Realistic Lens Design	22
3.3.1 Paraxial Design	22
3.3.2 Realistic System	22
3.3.3 Adding additional lenses	23
4 Results of Optical Design	27
4.1 Spot Size	27
4.1.1 Single lens	27
4.1.2 Lenslet Array	27
4.1.3 Spot Elongation	29
4.2 Wavefront Map	30
4.3 Aspherical Component	31
5 Conclusion	33
A Wavefront Maps	35

List of Figures

1.1	Artist representation of the ELT	1
1.2	Example of a distorted wavefront and where the Fried Parameter (r_0) can fit on the wavefront[16].	2
1.3	A figure showing a simulated source with different telescope diameters. As the telescope diameter gets larger, more "speckles" begin to appear [16].	2
1.4	Here we can see using the Speckle technique that there are actually two stars in what was previously believed to be one star.	3
1.5	Here we can see the clear difference between the AO corrected image and no AO correction.	4
1.6	Representation of Single Conjugate AO[2].	5
1.7	An example of a lenslet array with wavefront error.	5
1.8	An example of a pyramid wavefront sensor. The light from the aperture is focused onto the tip of the pyramid. From there, the light passed through the pyramid is relayed to the CCD. Wavefront correction is based off the intensity of each circle $I_{1,2,3,4}$ [20].	6
1.9	Here we can see an example of turbulence picked up by off axis-star but not the Reference star[2].	7
1.10	A figure of SLAO. Note where the laser light does not cover. This is the cone-effect, where there is residual turbulence not corrected[2].	7
1.11	A Figure of a laser tomography set up. Here two lasers measure two different layers and measured by two different WFS to correct a Ground conj. DM. [2]	8
1.12	A systematic representation of METIS including its proposed SLAO system [6]	9
1.13	Figure showing the end result of Benjamin Arcier's research.[3]	10
2.1	View of the Instruments on ELT's Nasmyth platform. Things to note are the PFS and METIS on the right. The SLAO system needs fit in between the PFS and METIS. [7]	11
2.2	A representation of the Annular mirror design. The green object represents the laser light and the red represents light from infinity. [3]	12
2.3	Profile of the cage support structure. Made by ITEM. [18]	13
2.4	Thorlabs translation stage. The specs of which can be found in Table 2.1. This was the stage chosen for the moving components of the high order mechanical design. [1]	13
3.1	A plot of laser distance versus Zenith angle. The red lines mark the 45 degree zenith angle equaling a distance of 127km	16
3.2	A plot of laser focal distance compared to the laser spot distance. The focal length of the ELT is subtracted to show the distance between the annular mirror and the laser focus.	17

3.3	A plot of the different positions of each plane after L1. Note that the pupil plane is constant.	19
3.4	A plot of the back focal distances of the laser spot after L2 with the focal length of L2 listed in the legend.	19
3.5	A drawing of the paraxial design. Note that after L2 the focus of the pupil is at infinity.	20
3.6	A diagram of the electric fields during the interaction with a medium [15].	20
3.7	Above is the extent of the Offner Relay design. The top right optic is the pick off mirror for the light coming from the laser. From there the image has a 2x zoom by this configuration. Note that for off-axis mirrors, ZEMAX constructs the entire mirror.	21
3.8	An image of the first focus after the Offner relay zoom. We can see that there is significant tilt in the focal plane where the color change is.	21
3.9	Paraxial layout of the built system.	22
3.11	An Example of splitting a lens into two different optical components.	23
3.12	An Example of how a system can "blow up" without the correct Merit Function.	24
3.13	An image of the last few optics in the system. Where the color changes from green to blue is a rough indicator of where the pupil plane is.	24
3.14	A layout of the in line WFS.	24
3.15	A layout of the HARMONI WFS. In here the use a telescoping mirror system labeled as Altitude Focus Unit [9].	25
3.16	A layout of the METIS SLAO altitude compensator.	25
3.17	A layout of the full METIS SLAO design.	26
4.1	A figure of both fields having the spots within the Airy Disk.	28
4.2	A Figure with the calculated Airy Disk radius in the data sheet on the bottom left. The coordinates in the top left are displayed in microns. It should be noted that there is some aberration effect taking place.	28
4.3	Here a side by side comparison of two different field angles and their spots. Obviously the spots are too small to see anything revealing.	29
4.4	A figure showing an example of what causes spot elongation [17]	30
4.5	80km [14]	30
4.6	105km [14]	30
4.7	160km [14]	30
4.8	Here is a map of the wavefront at the lenslet array. PTV = 234 nm ; RMS = 52.6 nm.	31
4.9	A Figure showing a surface map of the aspherical component.	32
A.1	All wavefront maps for on axis and off axis spots at different Zenith angles	35

List of Tables

2.1	Spec table for the Thorlabs 220mm translation stage. [1]	14
3.1	Table of key dimensions of the SLAO system. For simplicity sake, the distance between the telecentric lens and the lenslet array is 0 in ZEMAX.	22

List of Abbreviations

ELT	Extremely Large Telescope
PSF	Point Spread Function
METIS	Mid-infrared ELT Imager and Spectrograph
DM	Deformable Mirror
AO	Adaptive Optics
SCAO	Single Conjugate Adaptive Optics
SLAO	Single Laser Adaptive Optics
LTAO	Laser Tomography Adaptive Optics
GLAO	Ground Layer Adaptive Optics
MCAO	Multi-Conjugate Adaptive Optics
MOAO	Multi-Object Adaptive Optics
NGS	Natural Guide Star
LGS	Laser Guide Star
WFS	WaveFront Sensor
PWS	Pyramid Wavefront Sensor
SHWFS	Shack-Hartmann Wavefront Sensor
MICADO	Multi-AO Imaging Camera for Deep Observations
HARMONI	High Angular Resolution Monolithic Optical and Near infrared Integral field spectrograph
PFS	Pre-Focal Station
MLA	Micro-lens Array

Dedicated to my friends and family who helped keep me going.

Chapter 1

Introduction

Contents:

1.1	History of Adaptive Optics	2
1.2	Single Conjugate Adaptive Optics	4
1.3	Single Laser Adaptive Optics	5
1.4	Laser Tomography Adaptive Optics	7
1.5	METIS Science Goals	8
1.6	Focus of the Thesis	9

The advancement of Astronomy has always been closely linked to achieving higher resolution. Early on, this was a conceptually easier. The bigger your telescope aperture, the more light can be collected. With early telescopes this was limited by how large of lens a manufacturer could make. Eventually lenses became so large that they can collapse under their own weight. Next, a way to make mirrors that did not tarnish too quickly became available. Mirrors could be supported from the back, allowing for large mirrors. When single mirror systems became too heavy, segmented mirror designs were created in order to have an almost limitless aperture size.



FIGURE 1.1: Artist representation of the ELT

However, the Earth's atmosphere interferes with light, widening the PSF of an object. This is also known as seeing limited observations. Now with the new generation of 25+ meter telescopes, a way to make diffraction limited observations is more necessary than ever. Wavefront errors can be calculated using the "Fried Parameter"

or r_0 . r_0 is defined as the largest distance on a telescope primary over which the phase of an incoming wave is well-correlated (Figure 1.2) [16]. The Fried Parameter at good sites is roughly equal to 10 to 15 microns [16]. As telescope diameters become larger than the Fried Parameter, more "speckles" start to develop (Figure 1.3).

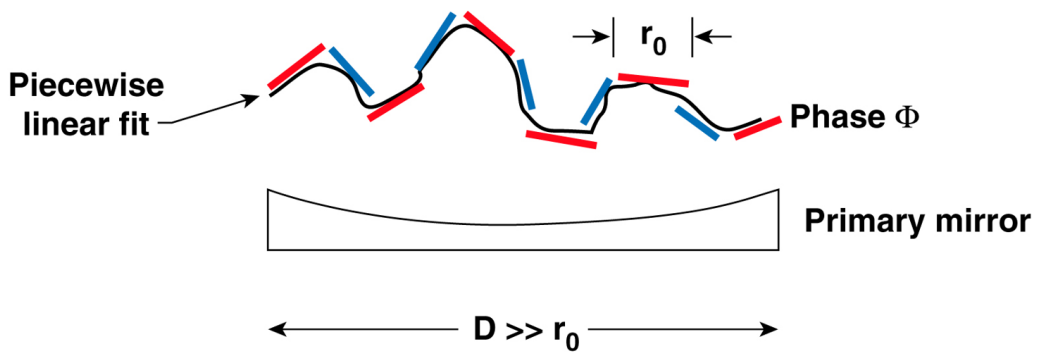


FIGURE 1.2: Example of a distorted wavefront and where the Fried Parameter (r_0) can fit on the wavefront[16].

The goal of any instrument is to achieve the highest possible "Strehl ratio". The Strehl ratio is defined as "the ratio of the peak aberrated image intensity from a point source compared to the maximum attainable intensity using an ideal optical system" [19]. Adaptive optics is the use of matching the wavefront errors with deformable mirrors to increase the Strehl Ratio of a given observation. The Mid-Infrared ELT Imager and Spectrograph or METIS, looking to take advantage of the ELT's 39 meter aperture to explore the mid-infrared sky. In order to do so, METIS must perform wavefront sensing to control the adaptive secondary.

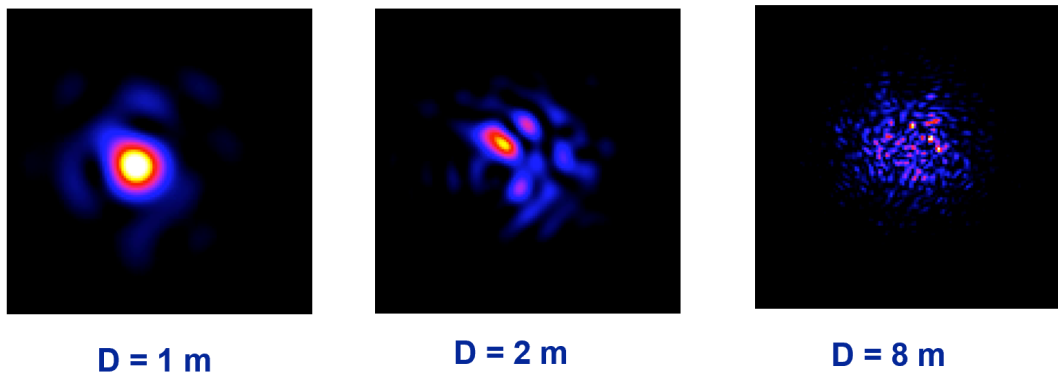


FIGURE 1.3: A figure showing a simulated source with different telescope diameters. As the telescope diameter gets larger, more "speckles" begin to appear [16].

1.1 History of Adaptive Optics

Light observed from astronomical sources travels anywhere from light years to billions of light years to our ground based detectors. Usually travelling mostly unimpeded through out that entire journey. Most of the distortion comes from the last

100 kilometers when the wavefront interacts with the atmosphere. The change from vacuum to the medium that is our atmosphere causes the light to refract. However, the atmosphere is not homogeneous. The atmosphere has temperature fluctuations and mixing currents that cause difference in indices of refraction and path length of incoming light.

Now that telescopes can be made to be eight meters and bigger, being able to correct for the Earth's atmosphere is necessary to advance ground based astronomy. First attempts to get around the atmosphere's interference with incoming light was the speckle imaging technique. The idea was to take short exposures of the target in order to limit the effects of the atmosphere.

Speckle imaging allowed for countless discovery of binary star systems that were otherwise observed as singular stars. This lead to the discovery of multiple binary star systems that were otherwise assumed to be one star (Figure 1.4). One particular method was called the "Shift-and-Add" Method. This method incorporated taking multiple short exposures and aligned images based on the image centroid and added the images together, usually giving an overall lower Strehl ratio [4]. However, this technique could only be used on bright objects. This means that there is still a large part of the night sky that we cannot observe using this technique.

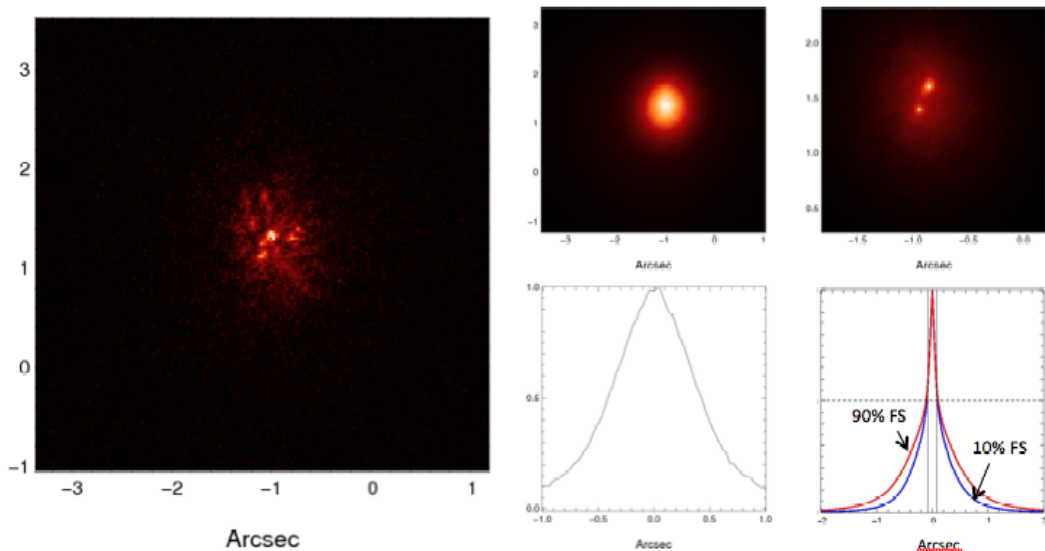


FIGURE 1.4: Here we can see using the Speckle technique that there are actually two stars in what was previously believed to be one star.

In order to advance imaging techniques, it became necessary to reconstruct the wavefront as it was before it encountered the atmosphere. Because the atmosphere distorts the wavefront, it should be feasible to match the wavefront to correct for the aberrations to the wavefront. This is done by having a deformable, reflective membrane. These are called deformable mirrors (DM). DM's are responsible for reconstructing the wavefront errors in the atmosphere to counter the phase differences, thus reconstructing the image (Figure 1.5).

In order for DMs to accurately match the wavefront error, there needs to be an additional calibration source. This can be done a few ways. The ways covered in this thesis will be Single Conjugate Adaptive Optics (SCAO), Single Laser Adaptive Optics (SLAO), and Laser Tomography Adaptive Optics (LTAO).

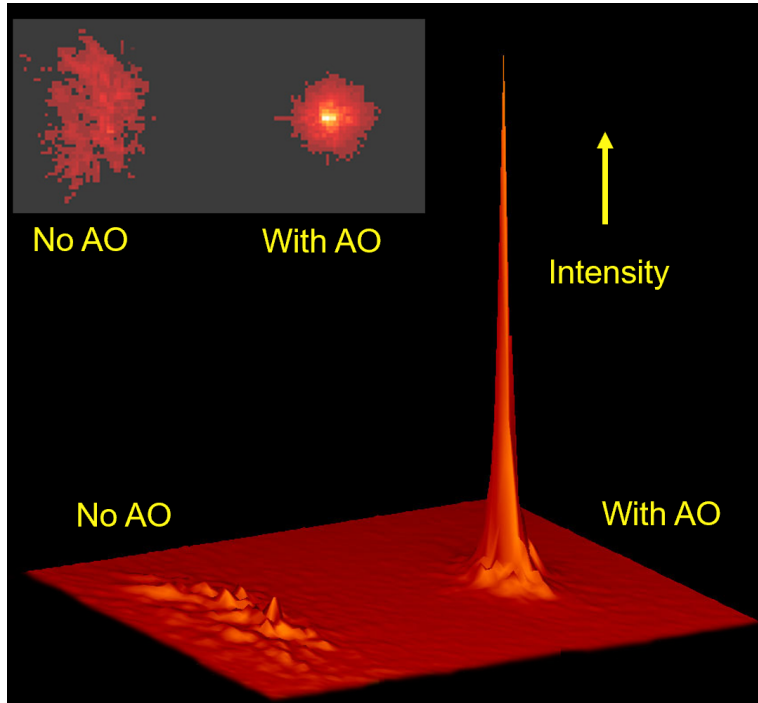


FIGURE 1.5: Here we can see the clear difference between the AO corrected image and no AO correction.

1.2 Single Conjugate Adaptive Optics

Adaptive Optics, in order to work, needs a reference source to measure the disturbances of the Earth's atmosphere. In this case, we look at a Natural Guide Star (NGS). An NGS is a sufficiently luminous star that can be used for wavefront detection. In the case of METIS, it was determined that a magnitude 10 star in the K-band would be needed for sufficient wavefront correction [5]. The sufficiently bright star properly illuminates the entrance pupil to be measured by a wavefront sensor (WFS). Currently there are two methods to measure wavefront error (Figure 1.6).

First is a Shack-Hartmann Wavefront sensor. This method uses a lenslet array to subdivide the pupil plane to measure deviations from a planar wavefront. This is done by measuring deviations from a grid of spots created by the lenslet array (Figure 1.7). This is the current method the METIS SLAO system will be incorporating to do wavefront sensing and will be covered in Chapter 3.

The second is a Pyramid Wavefront Sensor (PWS). PWS works by focusing light of the focal plane onto the tip of a pyramid to subdivide the aperture into four segments. The detector is placed at the pupil plane and directly images the pupil (Figure 1.8). The advantage of a PWS is that the light is divided only four times. This means that the NGS can be a higher magnitude and still allow for AO corrections [20]. The METIS SCAO system will implement a PWS inside of the cryostat[8].

One of the big advantages of Single conjugate AO is that star light comes from outside the Earth's atmosphere. This means that, to first order, wavefronts are planar and that the same source can be used for tip/tilt measurements. This will be an issue when using Laser Guide Stars (LGS). One thing effects SCAO systems is anisoplanatism. This is when a NGS is off-axis from the observed object. This will lead to residual wavefront error that is not in line with the observed object since the

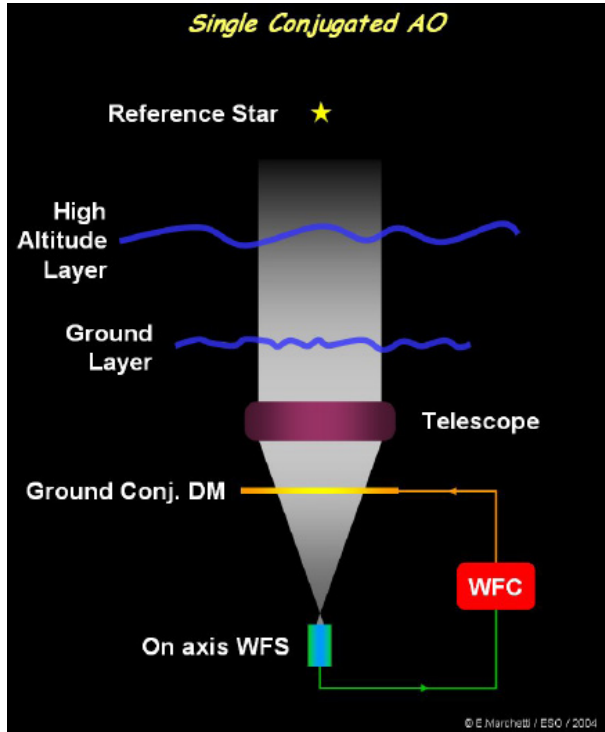


FIGURE 1.6: Representation of Single Conjugate AO[2].

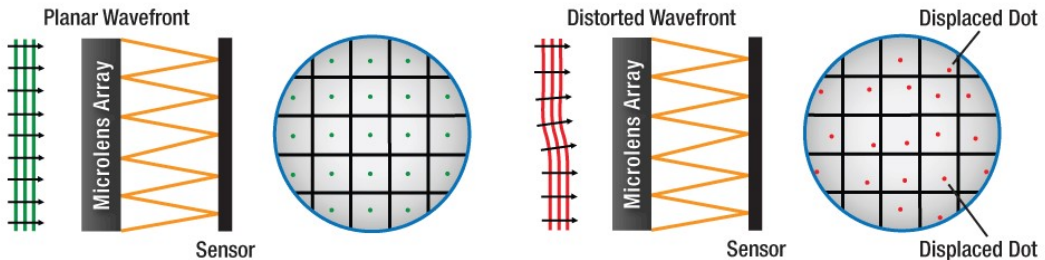


FIGURE 1.7: An example of a lenslet array with wavefront error.

two different sources go through different parts of the Earth's atmosphere. This is illustrated in Figure 1.9.

However, the night sky is not filled with sufficiently bright stars. Especially for extra-galactic observations, there is a need for bright sources. An artificial star is necessary for these types of observations. This is where laser guide stars come in.

1.3 Single Laser Adaptive Optics

Single laser Adaptive Optics (SLAO) is the practice of using a Laser Guide Star (LGS) in order to illuminate the night sky to have enough illumination on the entrance pupil of the telescope. Nowadays, the main type of laser used in astronomical adaptive optics is the sodium laser. The top of the Earth's atmosphere has a 10 km thick layer of sodium approximately 90 km above sea level [17]. This is the highest altitude an artificial star can be. The other laser type, the Rayleigh, laser has a height of roughly 20-40 km above sea-level [22].

Sodium lasers excite sodium atoms in the upper atmosphere and emit at 589 nm. The advantage of having the laser higher in the atmosphere is that it limits the cone

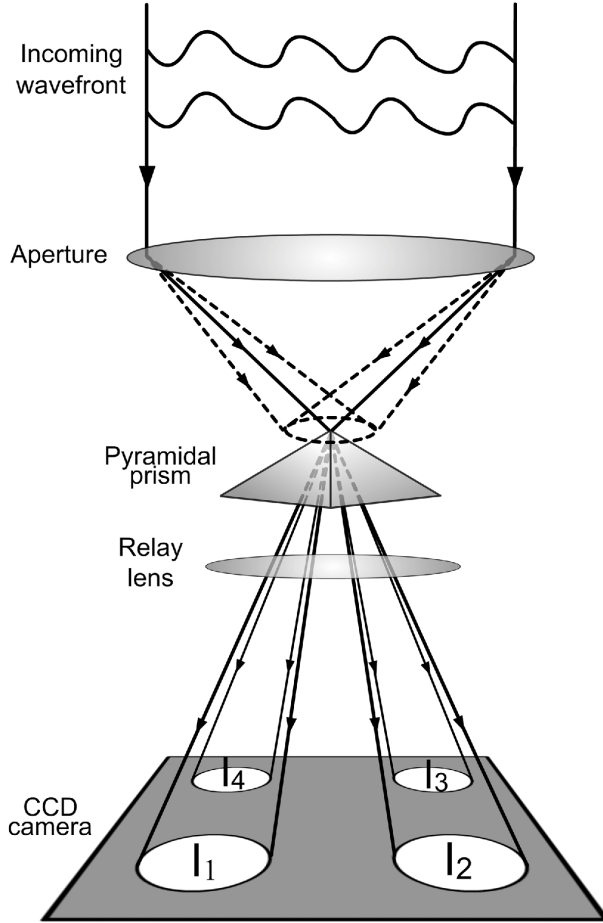


FIGURE 1.8: An example of a pyramid wavefront sensor. The light from the aperture is focused onto the tip of the pyramid. From there, the light passed through the pyramid is relayed to the CCD. Wavefront correction is based off the intensity of each circle $I_{1,2,3,4}$ [20].

effect. The cone effect is where there is residual turbulence not picked up by the laser spot (Figure 1.10). This is not always a full proof method though. The sodium layer is not a uniform and constant layer. On a time scale of hours, the thickness, height, and density of the sodium layer can change [17]. This will lead to variations in intensity of the LGS.

Laser guide stars also are not capable of providing tip/tilt measurements. This is due to the fact that the laser both travels up and back down in the atmosphere. This means that an off-axis star is required to provide tip/tilt measurements. However, the star can be higher in magnitude since the star is not needed for wavefront correction.

While taking an AO class with Claire Max at UC Santa Cruz, she described SLAO is "like looking through a straw". The correction done by SLAO provides correction but for a small FoV. This is in part due to the cone effect of SLAO observations. New techniques have come about to limit the cone effect and expand the FoV for laser AO systems. Some examples are Ground Layer AO (GLAO), Multi-conjugate AO (MCAO), Multi-Object AO (MOAO), and Laser Tomography AO (LTAO). METIS was originally designed for LTAO corrections.

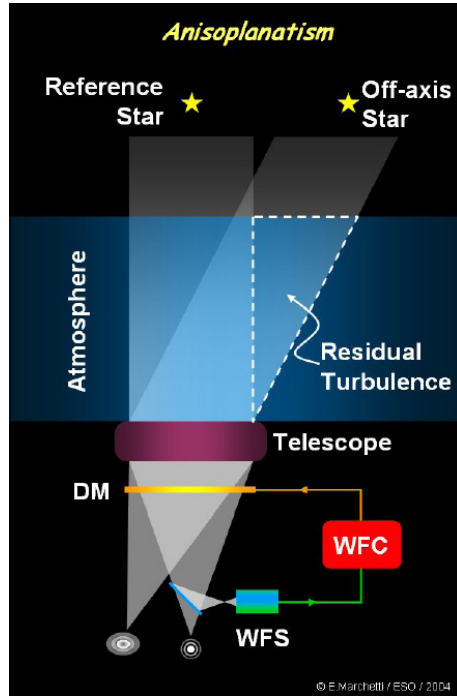


FIGURE 1.9: Here we can see an example of turbulence picked up by off axis-star but not the Reference star[2].

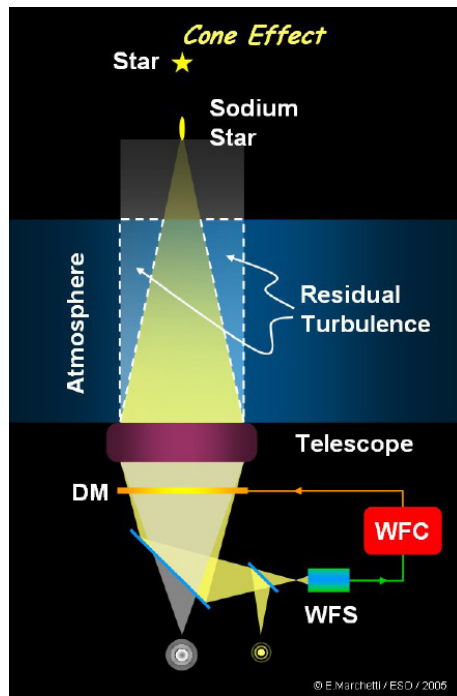


FIGURE 1.10: A figure of SLAO. Note where the laser light does not cover. This is the cone-effect, where there is residual turbulence not corrected[2].

1.4 Laser Tomography Adaptive Optics

Laser Tomography Adaptive Optics (LTAO) is the practice of using multiple LGS to illuminate a single conjugate plane. Each laser samples a different portion of the

plane and reconstructs the whole plane after the signal is combined by the WFS. This helps prevent the cone effect and enable better on-axis performance [2]. Each laser has an associated WFS to sample a part of the plane. ELT has 6 LGS, which would mean 6 WFS. This can lead to more time, money, and space to implement a LTAO system. All of which are critical aspects of any project. LTAO does provide better performance with wavefront reconstruction as well as widening the FoV of observations. An illustration of LTAO can be seen in Figure 1.11.

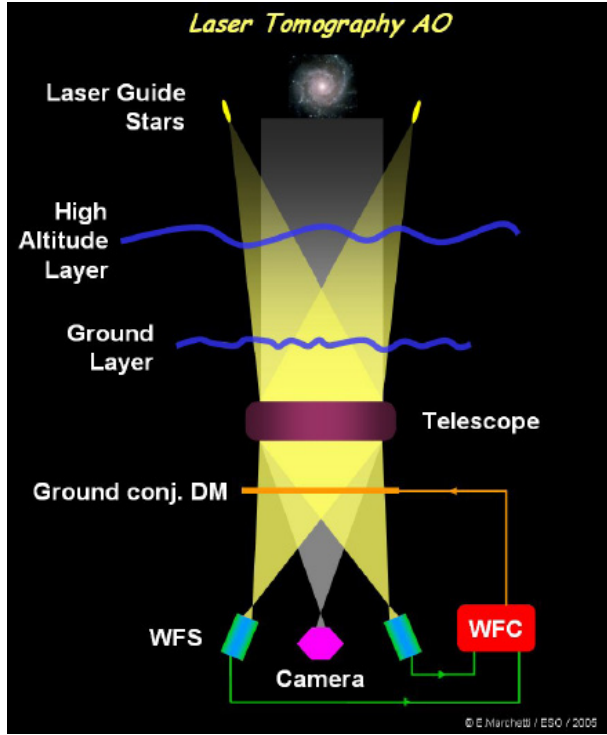


FIGURE 1.11: A Figure of a laser tomography set up. Here two lasers measure two different layers and measured by two different WFS to correct a Ground conj. DM. [2]

1.5 METIS Science Goals

The Mid-infrared ELT Imager and Spectrograph (METIS) goal is to explore the L-($2.9\text{-}4\mu\text{m}$), M-($4.6\text{-}5\mu\text{m}$), and N-($7.5\text{-}13\mu\text{m}$) bands using the Extremely Large Telescopes (ELT) 39 meter aperture. The main goal for METIS is to explore proto-planetary regions. This allows for the central star to be used as the main source for wavefront detection. A layout of MEITS can be seen in Figure 1.12. However, METIS can be used to explore many regions of the night sky outside of exo-planet discovery. Because METIS will be one of the few instruments with mid-IR seeing, it would be of great benefit to have METIS observe extra-galactic objects. These observations would more than likely require the use of a laser guide star (LGS) in order to do wavefront sensing. Originally it was thought that METIS would use the full suite of lasers that comes with the ELT, however due to constraints in budget, size and weight, it was considered looking into whether or not using a single laser would be just as effective.

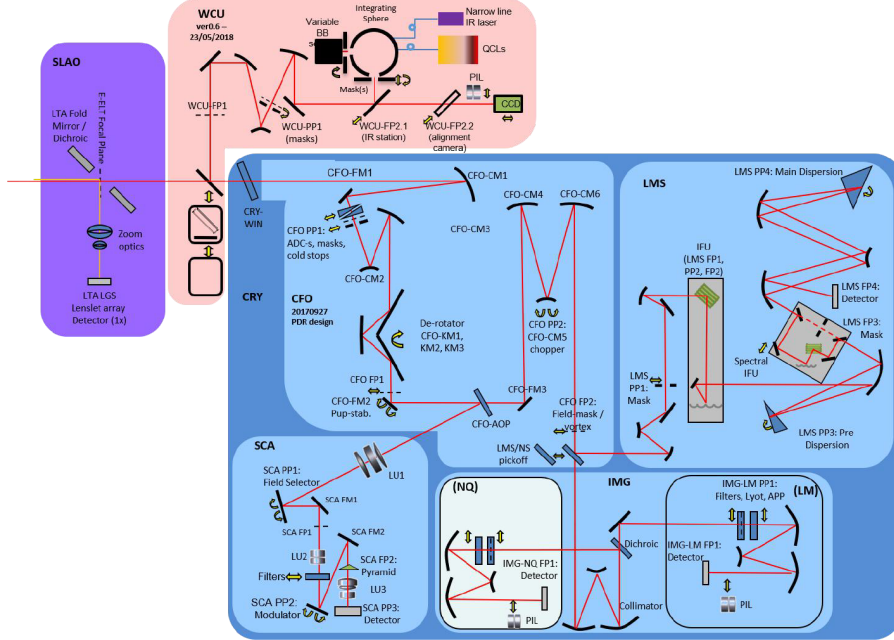


FIGURE 1.12: A systematic representation of METIS including its proposed SLAO system [6]

The advantages of using a single laser are that the cost would be dramatically reduced only sensing one layer rather than having multiple wavefront sensors. Having multiple wavefront sensors means more optics, which entails more space and more cost. The size limitations to the wavefront sensor are from the position of METIS from the pre-focal station of the ELT Nasmyth platform.

Because METIS is an infrared instrument, we need to pick off the incoming laser light with the use of as little optics as possible. This is because each optic has an associated temperature to it. Therefore, each optic can potentially add noise to the system. Using a beam-splitter dichroic is one option. The idea would be that the dichroic would allow the infrared light to pass through while sending off the light from the laser off to the wavefront sensor. However, since the SLAO system will be outside of the cryostat, the optic will be relatively warm. So any optics outside of the cryostat would significantly add to the noise of the instrument. Instead, we use the fact that the laser and the science objects will have different foci (this will be covered in greater detail in Section 2.1). The solution of an annular mirror was brought up. This would act as a beam-splitter, allowing the science light to pass through a central hole in a mirror while picking up off the light from the laser, sending it off to the wavefront sensor.

1.6 Focus of the Thesis

The new class of extremely large telescopes (25+ meter) needs to use adaptive optics in order to take advantage of the full aperture size. Originally, METIS was posed to use LTAO. However, since cost is always a large factor in any project, it was worth looking into using a SLAO system. This work was done by a previous student, Benjamin Arcier. His work showed a SLAO system for METIS could achieve a Strehl ratio of $\approx 60\%$ [3]. From this, an initial optical design was made and can be seen in Figure 1.13a. However, it was shown to be costly. The design had all aspherical

surfaces from large optics to very small. All of which are possible to make, however they are quite expensive due to the manufacturing process in which aspherical components are made. Spherical surfaces however are much cheaper to manufacture.

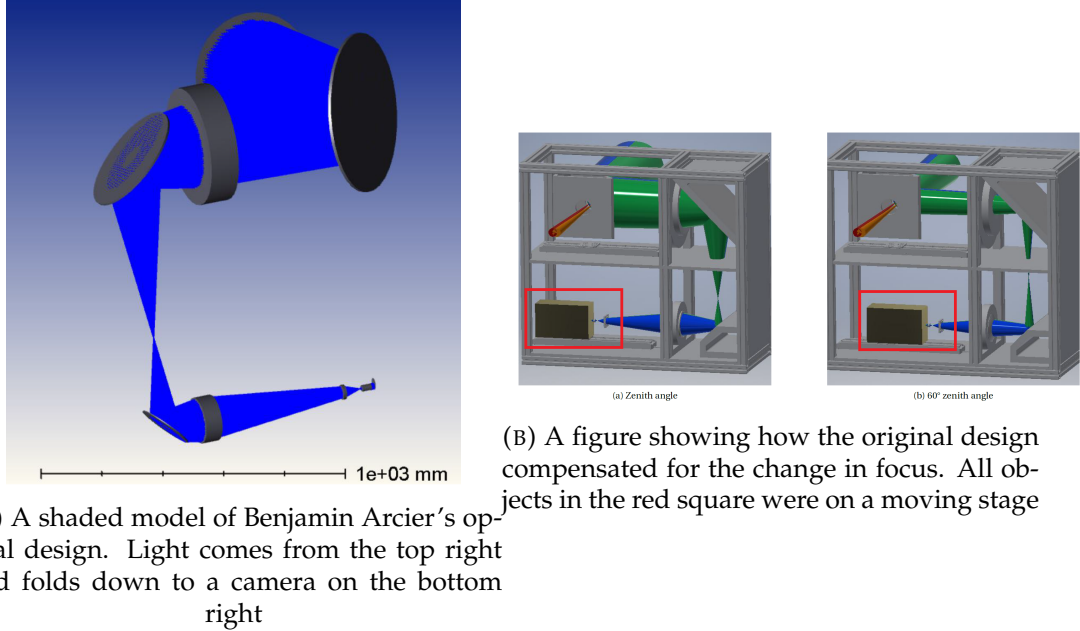


FIGURE 1.13: Figure showing the end result of Benjamin Arcier's research.[3]

Another issue was the way the system dealt with the change in focus from telescope elevation angle change. The design had the camera and two separate optics mounted to a moving platform to compensate for the changing distance of the laser spot. This presents a problem. With the camera attached to the moving stage, so does the additional cabling. This could wear down the cables insulation and could lead to failures. Because of this, it is important to implement a simple way to compensate for the change in laser distance with as few moving parts as possible.

The focus of this thesis is to explore these issues by looking at different optical concepts to produce a more manufactureable design. This included looking into mirrored systems for magnification and adding more optical surfaces to manipulate the light path. There should also be a simple mechanism to adjust for the change in focus of the laser spot with as few moving optical surfaces as possible. After the optical design is complete, the next step was to construct a first order opto-mechanical design to fit within the space envelope between METIS and the prefocal station of the ELT.

Chapter 2

Mechanical Design of Initial Optical Design

Contents:

2.1 Mechanical Constraints	11
2.2 Mechanical Components	12

Here I will go over the beginning of the project where myself and Benjamin Arcier worked in parallel.

2.1 Mechanical Constraints

The mechanical design for the SLAO system are constrained by the placement of METIS itself on the Nasmyth platform of the ELT. METIS will share the Nasmyth platform with two other instruments; **MICADO** (the Multi-AO Imaging Camera for Deep Observations) and **HARMONI** (High Angular Resolution Monolithic Optical and Near-infrared Integral field spectrograph). These three instruments will be positioned around a pre-focal station located at the ELT Nasmyth port as seen in Figure 2.1.

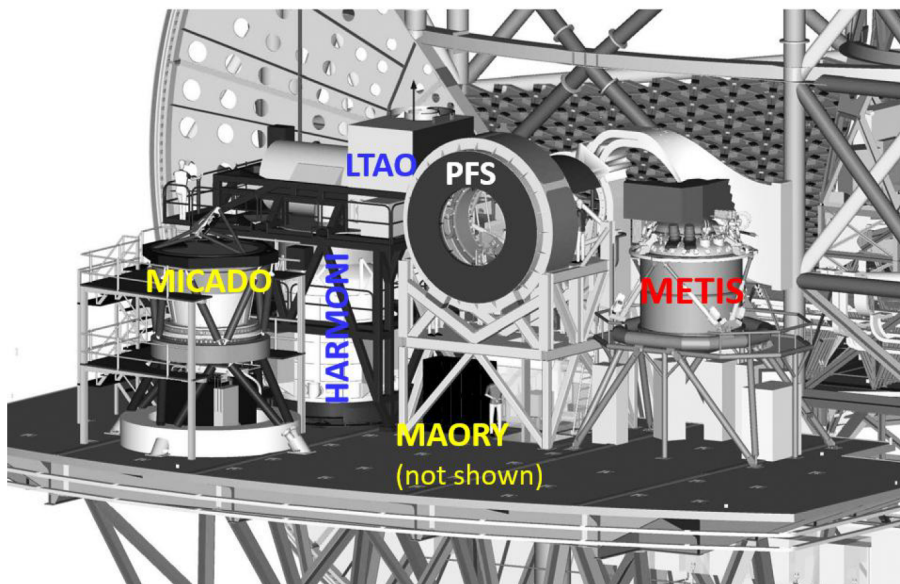


FIGURE 2.1: View of the Instruments on ELT’s Nasmyth platform. Things to note are the PFS and METIS on the right. The SLAO system needs fit in between the PFS and METIS. [7]

The structure of the SLAO system needs to fit in between the Pre-focal station and METIS itself. Therefore, the more compact the structure is, the better. One of the main constraints is the width of the structure. This is dominated by the laser pick-off mirror. METIS, as previously discussed in Chapter 2, is a mid-infrared instrument. Because the SLAO system would be outside of the cryostat, a beam-splitter would radiate too much in the infrared. This would be a large source of noise and would not be an ideal solution. An ideal solution was researched in the report of Arcier 2018 of an Annular Mirror [3]. This would take advantage of the central obscuration (ELT M2) as well as the fact that the observed object and the laser spot are at different distances from the primary mirror. From this, dimensions for an annular mirror were made to pickup laser light while allowing the science image to pass through (Figure 2.2).

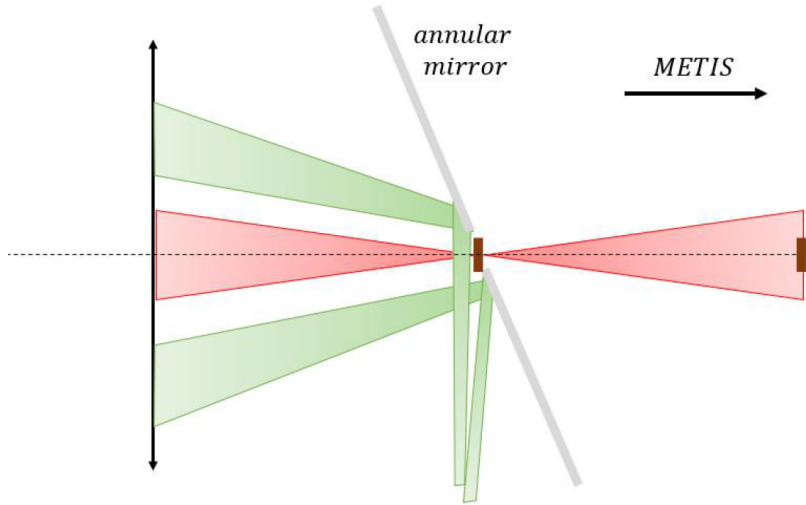


FIGURE 2.2: A representation of the Annular mirror design. The green object represents the laser light and the red represents light from infinity. [3]

This is where the annular pick-off mirror will be placed. This will be covered in finer detail in Chapter 3. What this means for the opto-mechanical design is that the diameter of the annular mirror drives the width dimension. The radius calculated by ZEMAX of the mirror is 240mm, which gives a width of $2 \times r \times \cos(45) \approx 340\text{mm}$. From there, light converges and the optics get smaller. To make the SLAO system more compact, we implemented fold mirrors to angle the light.

2.2 Mechanical Components

With the light path folded into a manageable profile, the next task was to design a cage around the optics. The cage supports were taken from the manufacturer ITEM. The selected profile was chosen due to it having the least amount of sag for the weight of the largest optic [18]. From this profile, the cage was designed to have a total dimension of $1.2m \times 1.2m \times 400mm$. The profile of the support structure can be seen in Figure 2.3.

Next, the design called for two moving stages. One for the annular mirror to move out of the light path for SCAO observations, the other for the altitude compensator stage. Benjamin Arcier's optical design had a range of travel equal to



FIGURE 2.3: Profile of the cage support structure. Made by ITEM.
[18]

182.178mm. Therefore, a stage that could handle both moving the annular mirror out of the way as well as for altitude correction would be ideal. The Thorlabs 220mm translation stage was chosen. The stage had the range of travel needed for both moving stages and had a desirable accuracy for the altitude correction. I will go further into altitude correction in Section 3.1. Though the horizontal loads limit is quite low, this will not be a problem since all moving stages were placed to move normal to gravity. The translation stage also had a small breadboard attached to it for mounting optics as seen in Figure 2.4. More specifications on the translation stage can be found in Table 2.1.



DDS220

FIGURE 2.4: Thorlabs translation stage. The specs of which can be found in Table 2.1. This was the stage chosen for the moving components of the high order mechanical design. [1]

With these components, a high-order cage system was designed for the optical design. Although the optical design had less than desirable characteristics (Section 1.6), we could prove that a SLAO system could fit into the space envelope between METIS and the PFS of ELT. The next step would be to find a more cost effective optical design to demonstrate to ESO that a more cost effective alternative to a LTAO

system is feasible.

Travel Range	220mm
Max Velocity	300mm/s
Min Achievable Incremental Movement	0.1 μ m
Bidirectional Repeatability	\pm 0.25 μ m
Horizontal Load Capacity (Max)	3.0kg
Actuator Type	Brushless DC Servo Motor
Cable Length	2.7m

TABLE 2.1: Spec table for the Thorlabs 220mm translation stage. [1]

Chapter 3

Optical Design

Contents:

3.1 Optical Constraints	15
3.1.1 Lenslet Array Calculations	16
3.1.2 Design of First Lens	17
3.1.3 The Rest of the System	18
3.2 Mirror Systems	19
3.3 Realistic Lens Design	22
3.3.1 Paraxial Design	22
3.3.2 Realistic System	22
3.3.3 Adding additional lenses	23

The main focus of this thesis was to explore different optical designs to reduce cost and make a SLAO system a more desirable option to ESO than an LTAO system. The first optical design (covered in Section 1.6) had three main lenses of varying size, all with aspherical surfaces. To make the SLAO system more desirable, optical components should be easy to manufacture and thus be cheaper. This chapter goes into the exploration of that goal.

3.1 Optical Constraints

In order to redesign a new system from scratch, it is important to understand what the system is supposed to do as well as what is constraining the system. First thing and maybe most importantly, is to focus the laser spot. The laser spot is a known distance from the telescope, therefore it will not be an infinity focus. We know that the sodium layer is roughly 90 km above sea-level with a approximate thickness of 10 km [17]. So for the telescope pointing at Zenith, we can assume that the laser spot is 90 km above the telescope. As the telescope changes zenith angle, the laser tracks the curvature of the Earth's atmosphere. So the distance of the laser spot can be computed as:

$$d_{LGS} = \frac{z_{LGS}}{\cos \zeta} \quad (3.1)$$

Where d_{LGS} is the distance of the laser guide star (LGS), z_{LGS} is the distance at zenith, and ζ is the angle away from zenith. The output of which can be seen in Figure 3.1. With this information we can calculate the difference in focal length between an object at infinity and the laser spot. First we take some approximations about the ELT itself:

1. Diameter (D) = 39m
2. $f/D = 17.48$
3. $f = 681.72m$

With this information we can do a first order approximation of where the focal point of an object will be using a simple formula:

$$\frac{1}{f} = \frac{1}{object} + \frac{1}{image} \quad \rightarrow \quad image = \left(\frac{1}{f} - \frac{1}{object} \right)^{-1} \quad (3.2)$$

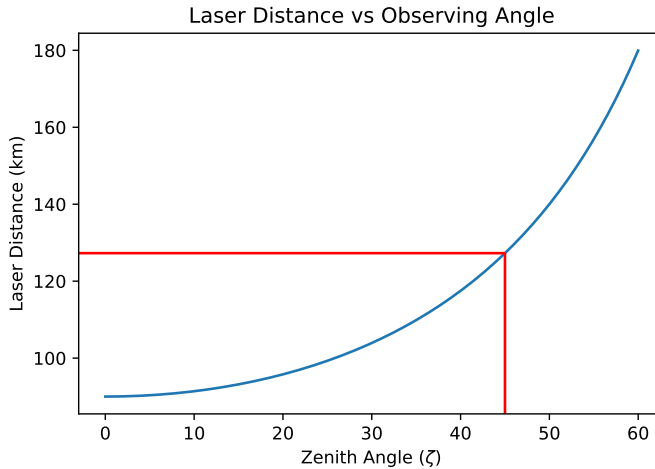


FIGURE 3.1: A plot of laser distance versus Zenith angle. The red lines mark the 45 degree zenith angle equaling a distance of 127km

For an object at infinity, this equation simplifies to $image = f$. Which in this case means the image is approximately 682 meters behind the primary mirror. This is where the annular mirror mentioned in Chapter 2 will be located. Next is to figure out how far back the laser light will focus. Since we can assume that the laser light will come to focus further than the science light, we can subtract the distance by 682 meters. This can be visualized by Figure 3.2.

3.1.1 Lenslet Array Calculations

On the other side, we need to know what we are imaging. First we note that the camera chosen for this system is a Large viSble cAmera (LISA) chosen by ESO that has a 800x800 pixel array with a pixel size of 24 microns. This gives a total array size of 19.2mm \times 19.2mm [10]. The lenslet array will need to have the following characteristics [3]:

- 40×40 subapertures
- 20 pixels per subaperture
- $10''$ FoV or $0.5''$ per pixel

The lenslet array needs to image directly onto the detector array to avoid any aberrations in the pupil plane. Therefore, the size of the lenslet array will need

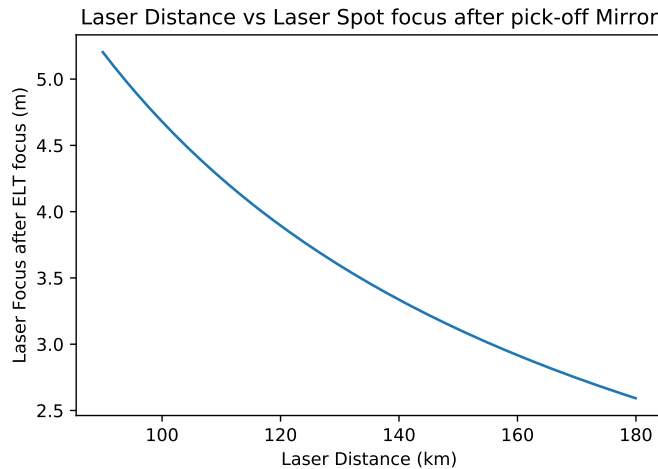


FIGURE 3.2: A plot of laser focal distance compared to the laser spot distance. The focal length of the ELT is subtracted to show the distance between the annular mirror and the laser focus.

to match the size of the detector array of 19.2mm. The lenslet will subdivide the pupil plane. So each lenslet will cover an equivalent of $39m/40 = 0.975m$ of the entrance pupil. This gives a diffraction limit for each lenslet to be $\theta = \lambda/d = 0.589\mu m/0.975m = 0.124''$. This gives the size of the Airy disk for each lenslet of $0.124''$. The pixel scale required is $0.5''/\text{pixel}$. This means that the pixel size will be ≈ 4 times the diffraction limit. This means that the pixel size needs to be $4 \times 0.589\mu m = 2.4\mu m$. Since the pixel size needs to be 24 microns, this means that the f -number will need to be equal to 10. The diameter of each of these lenslets will be $19.2mm/40 = 0.48mm$. Since we know what the speed of the lenslet should be, we can calculate the focal length of each lenslet:

$$f/D = N \rightarrow f = N \times D = 10 \times 0.48mm = 4.87mm \quad (3.3)$$

The key characteristics of the lenslet array are as follows:

- $f = 4.87mm$
- $D = 0.48mm$
- 40×40 array

3.1.2 Design of First Lens

Referring back to Chapter 2 again, we don't want to a system that is almost 5 meters long just to have the light come to focus. It is important that the first optic accelerate the light convergence in order to save space. For simplicity sake, we place our first lens one meter away from the annular mirror. We want the lens to have an F-number of roughly 3 ($f/D = 3$). So in order to do this, it was first necessary to find the diameter of the lens one meter away from the annular mirror. The laser spot size is the largest when the telescope is at zenith, therefore the calculations for this will be done at $\zeta = 0$. I wrote a small code to determine the size of L1 based on the focal length of the laser and the speed of a system. This uses the simple equation $f/D = N$ to determine D based on a distance behind the focal point.

```

def find_D(D,N,f1,f2):
    dist_new = f1 - f2
    D_new = dist_new / N
    return D_new

D_L1 = (find_D(D_elt,N_elt,laser_focus[0],dist_to_L1)).to(u.cm)
print(D_L1)

24.04584882426677 cm

```

This returned a diameter of 24 cm and from this we can calculate what the focal length of Lens 1 (L1) should be $f/D = N \rightarrow f = N \times D = 3 \times 24.05\text{cm} = 72.1\text{cm}$. With this focal length established, next is to find where the pupil plane is located and where the focal point is after L1.

3.1.3 The Rest of the System

With the constraints explained in Section 3.1 and Section 3.1.2, the rest of the system has a very straight forward approach to calculating the variables of each optic. First, we calculate the conjugate planes after L1. We can do this by using Equation 3.2 and the output from Figure 3.1.

We also want to know where the pupil plane is. Instead of taking the distance to the entrance pupil of ELT, we will use the distance from the exit pupil of the ELT. The exit pupil is defined as "the image of the aperture stop as seen from an axial point on the image looking through the interposed lenses [12]." Here the aperture stop is the primary mirror the ELT itself. According to ZEMAX, the exit pupil is located 38.349 meters away from L1. Since this location does not change with zenith angle, this distance will stay the same. The output of these different planes can be seen in Figure 3.3.

Next comes L2. L2 needs to focus the pupil plane to infinity. This is done by locating L2 one focal length away from the pupil plane. The reason the pupil plane should be focused to infinity is that the focal plane still varies in distance with respect to zenith angle. In the space between L2 and the next optic, L3, there can be an altitude compensator without impacting the image quality of the pupil plane. The focal length of L2 was not so fixed as the rest of the system. A few different focal lengths were tested and the output of which can be seen in Figure 3.4.

In Figure 3.4, there are a range of options for the focal length of L2. The choice came down to two factors: 1) The speed of the system, and 2) linearity. A focal length of 12.5 cm was deemed a good choice since it gave a f-number of 1.25, which is slow enough not to add too many aberrations and quick enough to make the system more compact, and the linearity of the range of focus is a nice thing to have.

The rest of the system was designed to do two things: 1) pass the light to a beam size that matches the size of the lenslet array, 2) and then create a telecentric lens that focuses the pupil image onto the lenslet array. Telecentricity is an optical property that has the pupil image suffer only from defocus and does not suffer from demagnification. The next step is to create an optical drawing of the system. Before looking into manufacturable optics, we can make an ideal approximation using a paraxial lens. The paraxial design was first drawn up (Figure 3.5) and then inserted into ZEMAX.

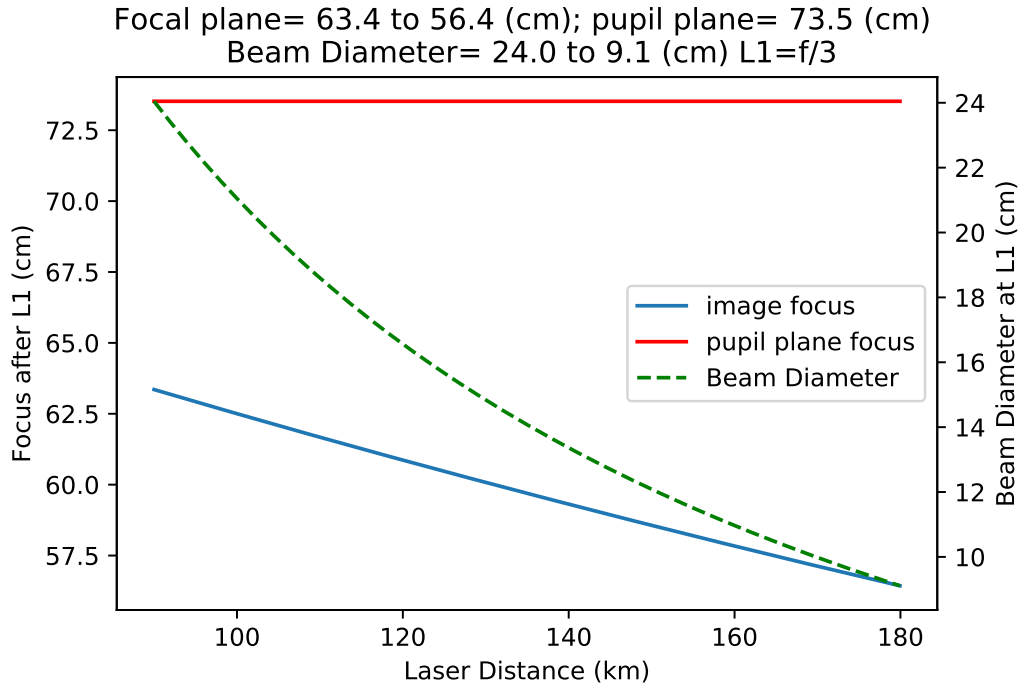


FIGURE 3.3: A plot of the different positions of each plane after L1.
 Note that the pupil plane is constant.

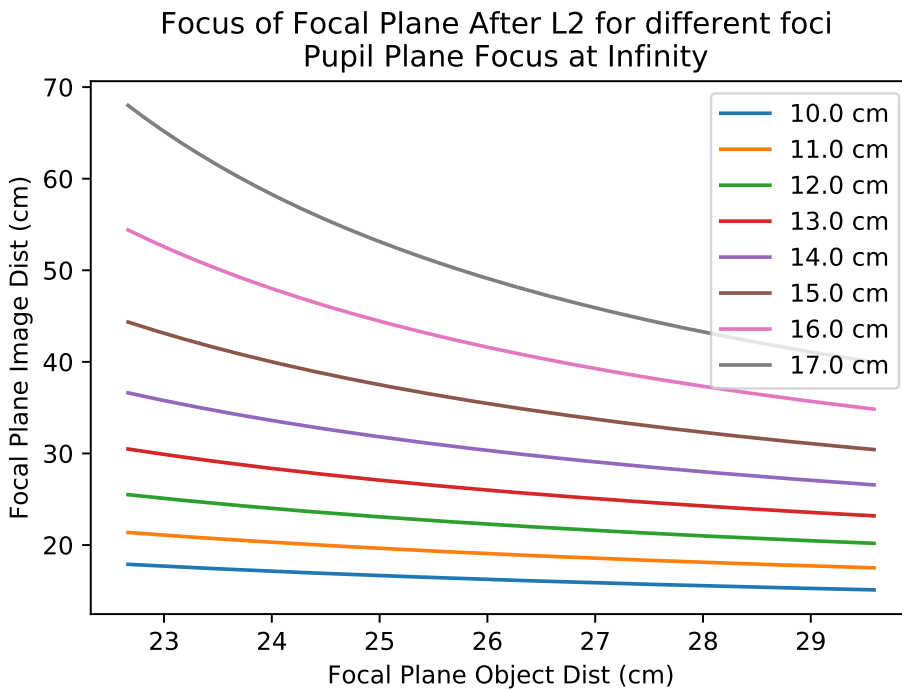


FIGURE 3.4: A plot of the back focal distances of the laser spot after L2 with the focal length of L2 listed in the legend.

3.2 Mirror Systems

The first option explored was to use mirror designs. The use of mirrors has the added benefit of having zero photon loss. As seen in Figure 3.6, the electric field

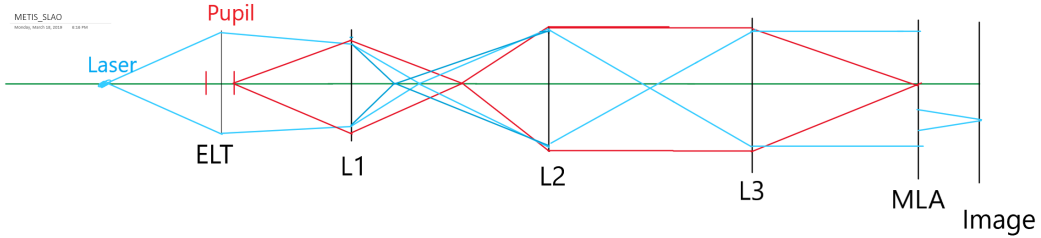


FIGURE 3.5: A drawing of the paraxial design. Note that after L2 the focus of the pupil is at infinity.

of the system can be broken down into the incident electric field (E^i), the reflected electric field (E^r) and the transmitted electric field (E^t). Using conservation of energy we can get the following equation:

$$E_0^i + E_0^r - E_0^t = 0 \quad (3.4)$$

With mirrors, the transmission component is zero, therefore the transmitted electric field is equal to the incident electric field ($E_0^i = E_0^r$). Mirrors also have the advantage of having more mechanical support since it is possible to mount mirrors on the back.

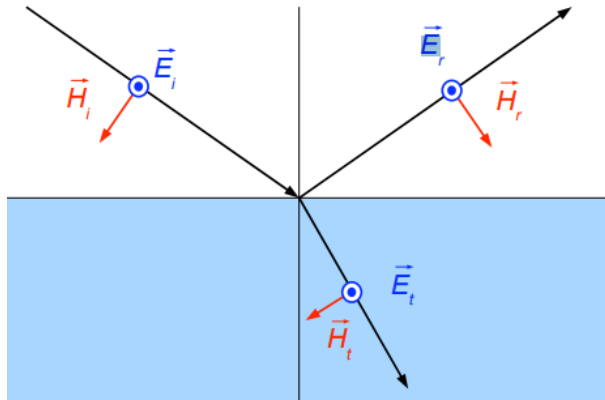


FIGURE 3.6: A diagram of the electric fields during the interaction with a medium [15].

The first design looked at was using an Offner relay to zoom the pupil plane. The design seen in Figure 3.7 was the resulting Offner relay. The initial resulting image (Figure 3.7), initially shows to have tilt in the image. In ZEMAX each field can have its own color associated to it. While it is not an exact indicator, the change in color gives an approximation of the image plane. This is because the entrance pupil picks up the two fields at the same time, side by side. So when the color changes, this is representative of the two fields changing positions.

The motivation behind the Offner relay was that it was a simple way to zoom the pupil image while taking up the least amount of space. However this soon became apparent that this design was not worth pursuing. While Offner relays offer good zoom depending on the placement of the mirrors, the change in focal length. In order to correct for this, there would have to be additional optics. This is due to the fact that we want the pupil plane at the lenslet array to be as flat as possible. These additional optics would more than likely add to the physical dimension of the SLAO system.

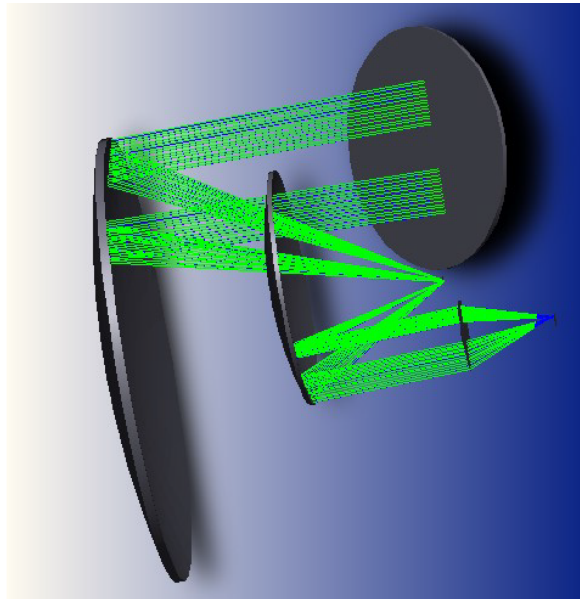


FIGURE 3.7: Above is the extent of the Offner Relay design. The top right optic is the pick off mirror for the light coming from the laser. From there the image has a 2x zoom by this configuration. Note that for off-axis mirrors, ZEMAX constructs the entire mirror.

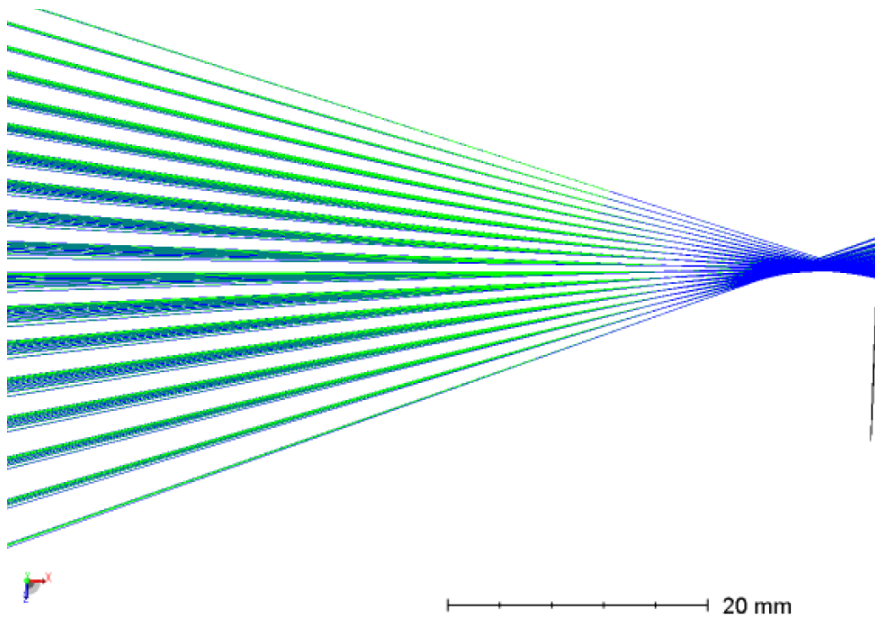


FIGURE 3.8: An image of the first focus after the Offner relay zoom. We can see that there is significant tilt in the focal plane where the color change is.

Other designs were looked into, such as a Gregorian zoom system as well as off axis parabolas in order to work in the space envelope. But all showed similar issues with space and tilt of the planes. Because of this, going back to a full lens system was deemed necessary and potentially simpler. However, this required some design changes from the original design. The goal of this design was to have an optical layout with all spherical surfaces. Also due to the fact that we are only dealing with one wavelength (595nm), the design could be made with only one glass type.

3.3 Realistic Lens Design

Here I go through the steps necessary to reach a manufacturable optical system.

3.3.1 Paraxial Design

A paraxial approximation is another version of the small angle approximation, where a ray angle $\theta \approx \tan \theta$ [11]. More simply put, this is the approximation of an ideal lens with no thickness and no radius of curvature, just a focal length. With the data from Section 3.1, we can make a table of each lenses attributes as seen in Table 3.1. Next, the data is applied into to get Figure 3.9.

Object	f	Lens Diameter	Distance to next object	N
L1	72.1 cm	24 cm	86 cm	3
L2	12.5 cm	10 cm	varying	1.25
L3	15.0 mm	50 mm	100 mm	3
Tele	-60 mm	19.2 mm	0	-
LA	4.87 mm	19.2 mm	4.87 mm	10

TABLE 3.1: Table of key dimensions of the SLAO system. For simplicity sake, the distance between the telecentric lens and the lenslet array is 0 in ZEMAX.

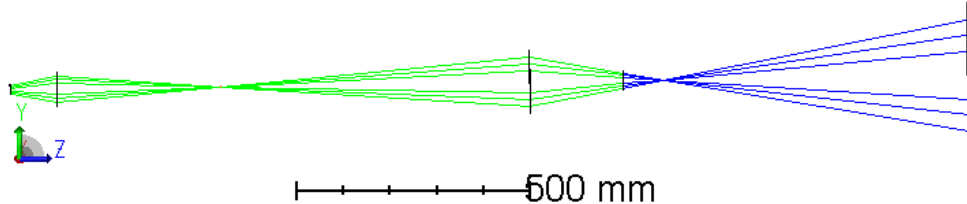


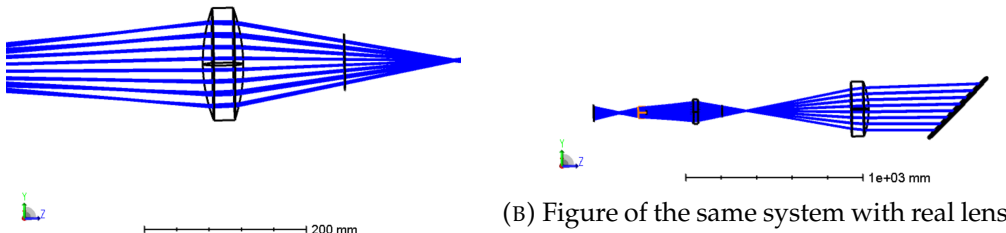
FIGURE 3.9: Paraxial layout of the built system.

3.3.2 Realistic System

With the paraxial system in place, next was to introduce optics that had the same characteristics as the paraxial lens. ZEMAX has a built in function that will allow a user to input a diameter and a focal length and will find an off-the-shelf part to match your specification. When inserting a manufacturable lens into ZEMAX, there are a few parameters that make up a basic lens:

1. Radius of curvature of each of the two lens surfaces
2. Thickness
3. Material

Zemax has the user build a surface based off of these parameters. A lens is made up of two surfaces (Figure 3.10a). With the introduction of more physical lenses, image quality and pupil quality. The next step is to construct a proper merit function to constrain the system and let the program optimize itself.



3.3.3 Adding additional lenses

Since the design was not working with substituting single lenses for paraxial ones, the next idea was to divide a single lens into two lenses by inserting two surfaces in the middle of a lens. This would allow ZEMAX to have additional variables at its disposal to better optimize the system. An example can be seen in Figure 3.11.

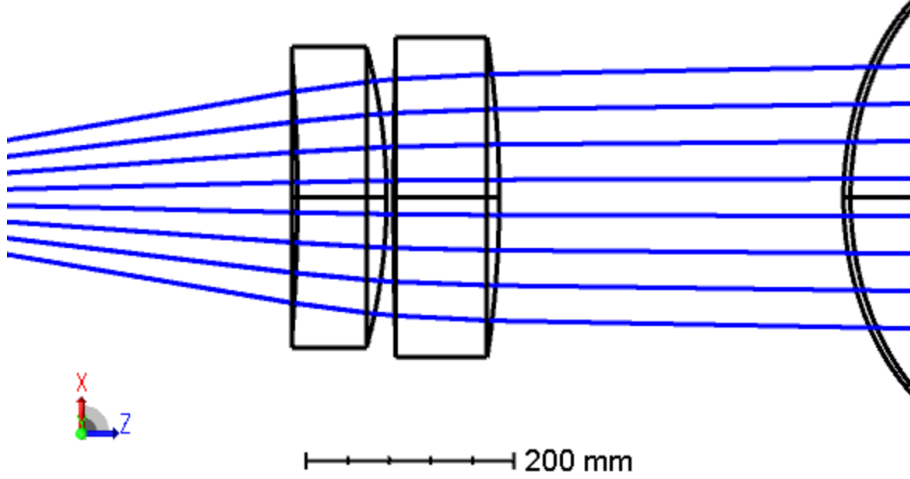


FIGURE 3.11: An Example of splitting a lens into two different optical components.

Now that the system has become more complicated, there needs to be more constraints on the system. ZEMAX, like most software, will not always do what you want it to at first. Unless otherwise specified, ZEMAX has no issue creating lenses inside of lenses and creating negative space in order to achieve the performance specified. As my advisor Remko Stuik said, "there are a million different ways that an optimization can go wrong, but only one way for it work correctly." The way to correctly optimize a system in ZEMAX is to build a merit function. There are a few things the Merit function was crucial in. First, the merit function allows the user to prevent unrealistic designs such as lenses within lenses and negative thicknesses. Second, it also allows you to place pupil and focal planes in certain locations. This was a crucial aspect of this design since the lenslet array needs to image the pupil plane. That means the pupil plane needs to land exactly on the face of the lenslet array. Lastly, the spot size. It is possible to have a system with excellent pupil quality. However, if the spot size is not diffraction limited then the system cannot provide accurate wavefront measurements.

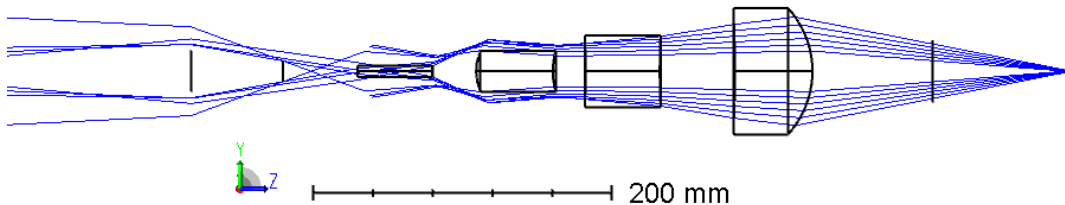


FIGURE 3.12: An Example of how a system can "blow up" without the correct Merit Function.

With a proper Merit function, designing a proper system was just an iterative process of optimizing, patience, understanding what had changed, and what function was driving those changes. After optimization, the system was not providing an acceptable wavefront in the pupil plane. The next step was to find where an aspherical surface could be located in order to provide the desired performance. This goes in contrast of the original goal of this thesis. Originally, the system was to have no aspherical lenses. However, having one aspherical surface could prove to be cheaper than adding additional optics that require space, and mounting. ZEMAX has a feature called "Find Best Asphere", where it goes through each optical surface and attempts to drive the Merit Function as low as possible. While running through the whole system would be a definitive way to determine the best surface, a close look at the system can show where the best surface would be (Figure 3.13).

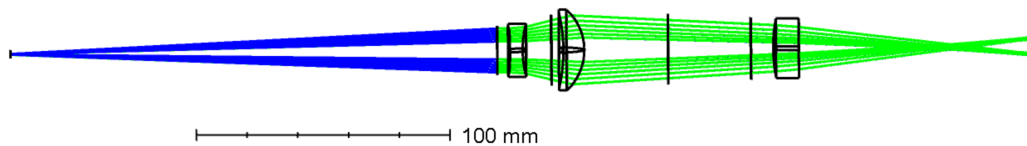


FIGURE 3.13: An image of the last few optics in the system. Where the color changes from green to blue is a rough indicator of where the pupil plane is.

In Figure 3.13, we can see where the pupil plane is. Here there is still a paraxial representation of the lenslet array. At this location there is still high wavefront error. The surface just before the lenslet array would be the ideal candidate. If the asphere could match the wavefront error, then there would be a flat wavefront reaching the lenslet array. To be safe, ZEMAX ran through each surface in Figure 3.13 to determine which was the best asphere. The back of the telecentric lens was indeed the best candidate. From that the inline design optimized to reduce the Peak-to-Valley (PTV) wavefront and drive the spot size down to the diffraction limit.

The design shown in Figure 3.14 showed that a design could be made to accurately do wavefront sensing with only one aspherical surface. The next step was to implement a simpler way to extend the light path for the changing laser distance.

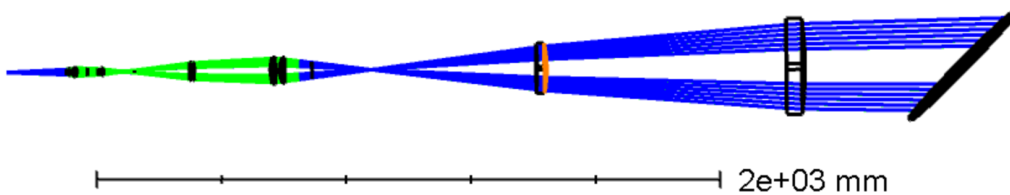


FIGURE 3.14: A layout of the in line WFS.

First, it is important to know where the light path can be extended without effect system performance. The pupil image quality is what needs to be preserved. Going back to Figure 3.5, we can see that the pupil image is focused to infinity between L2 and L3. This is where the system can correct for the changing laser distance. When looking at concepts to compensate for the changing altitude, we look to other instruments going onto the ELT. HARMONI implements a telescoping mirror system to extend the light path as seen in Figure 3.15.

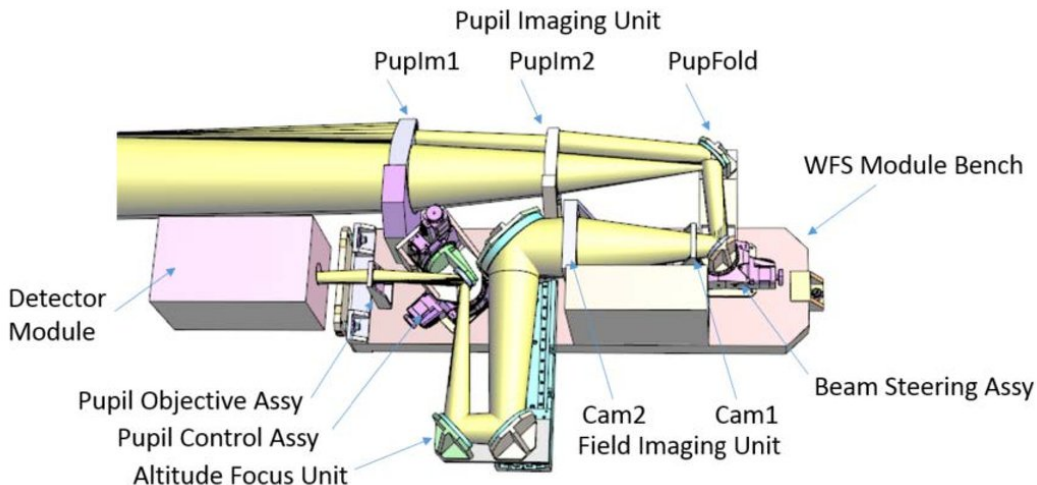


FIGURE 3.15: A layout of the HARMONI WFS. In here the use a telescoping mirror system labeled as Altitude Focus Unit [9].

A similar system was implemented in the design of the METIS SLAO system. This meant extending the distance between L2 and L3. However, with a stable merit function, this was easily implemented (Figure 3.16).

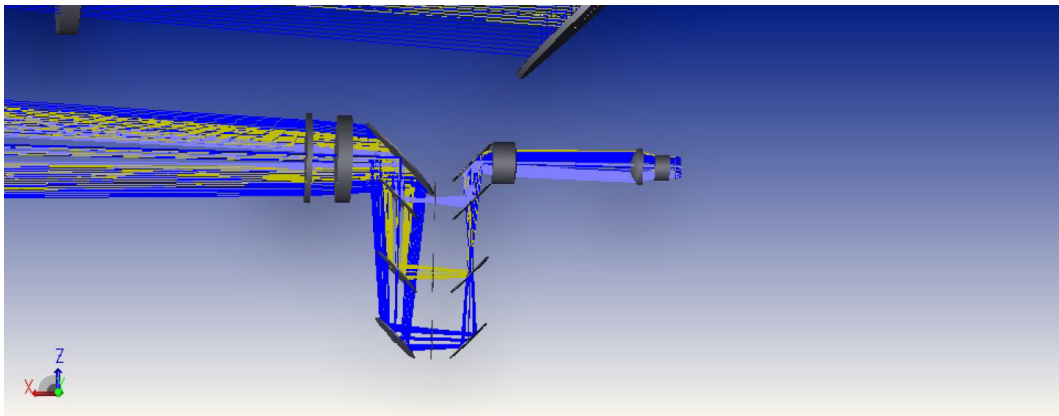


FIGURE 3.16: A layout of the METIS SLAO altitude compensator.

Next, the system needed to be more compact. One of the requests of the METIS SLAO system was to make the structure as compact as possible. The simplest way to achieve this was to add 45° fold mirrors in between the lenses. Flat, 45° mirrors only create coordinate changes, but do not effect the image quality. By adding the fold mirrors, the almost 3 meter long system was reduced to less than a meter long. The full system with fold mirrors and altitude compensator can be seen in Figure 3.17.

The last step was to replace the paraxial lenslet array. With the spot size and wavefront within tolerance, it was time to substitute in a realistic lenslet array. Adding

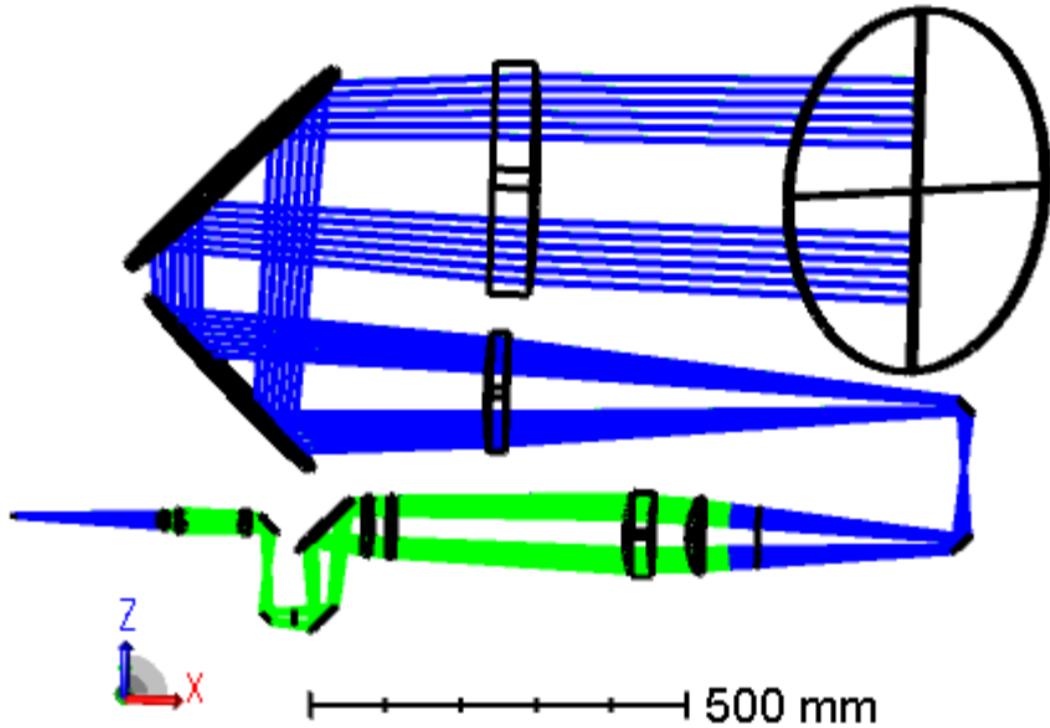


FIGURE 3.17: A layout of the full METIS SLAO design.

a lenslet array into ZEMAX can be done multiple ways. Normally ZEMAX allows for a non-sequential component to be added into a sequential system. The way to do this in ZEMAX is to select "Non-sequential Component" in the "Surface Type" section. From this you can open up the "Non-sequential Component Editor". In this you can normally add as many non-sequential components as you'd like. From there, an exit port surface needs to be made in order for ZEMAX to go back to calculating sequentially[13]. Despite making practice files and making them work outside of the system, it continued to fail when attempting to add it to the layout.

The next way was to use a "User Defined" surface. This option allows for the creation of a lenslet array in a sequential manner. However, this method does not allow for stable optimization in ZEMAX. The output from a lenslet array is of course, an array of spots. ZEMAX wants to have all of the rays through a pupil converge into one spot. Therefore, optimization was not an option. Using the calculations from 3.1.1, a lenslet array was designed from these parameters. From there, I used the slider function in ZEMAX to nudge the image plane after the lenslet array into focus. With the design in place, we can begin to look at the kind of performance it will achieve.

Chapter 4

Results of Optical Design

Contents:

4.1	Spot Size	27
4.1.1	Single lens	27
4.1.2	Lenslet Array	27
4.1.3	Spot Elongation	29
4.2	Wavefront Map	30
4.3	Aspherical Component	31

In this chapter I will go over the results of the finished Optical Design.

4.1 Spot Size

One of the requirements of an AO system is to be diffraction limited. One prerequisite is for the spot size to be smaller than the Airy Disk of the system. ZEMAX is able to display the Airy disk on spot diagrams. Since the system could not analyze a spot array, this section will look at the results from a single lens and then that of the lenslet array.

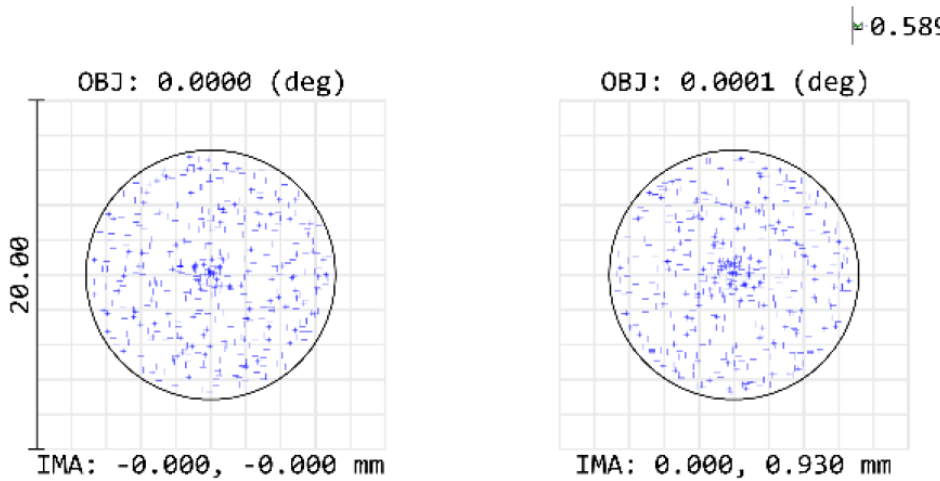
4.1.1 Single lens

Here, a single lens over the whole aperture was used in place of an MLA. This allowed for the system to optimize with a known spot size and allowing all of the rays that pass through the entrance pupil to converge in the image plane. A f/10 lens was put in place as a scale up of the lenslet. As the system optimized, eventually the spot size became smaller than the Airy Disk of the system, thus becoming diffraction limited.

As seen in Figure 4.1, the Airy disk has a radius of $7.159\mu m$, while the spot has an RMS radius of $4.571\mu m$. While the spot size could be improved, the wavefront error started to degrade as spot size decreased. Since we are only imaging spots and not looking for definition, this should still prove to perform just as well.

4.1.2 Lenslet Array

As described in Section 3.3.2, the lenslet array was designed based off hand calculations and focused by hand. The system did not go through an optimization process. So it is crucial to understand if the system is performing adequately. First, since the aperture size of the lenslet changed, so did too the radius of the Airy Disk. Only spots off-axis could be analyzed due to light being blocked by M2.



Surface IMA: Focus

Spot Diagram

7/6/2019
 Units are μm . Airy Radius: 7.159 μm . Legend items refer to Wavelengths
 Field : 1 2
 RMS radius : 4.571 4.636
 GEO radius : 6.872 6.755
 Scale bar : 20 Reference : Centroid

FIGURE 4.1: A figure of both fields having the spots within the Airy Disk.

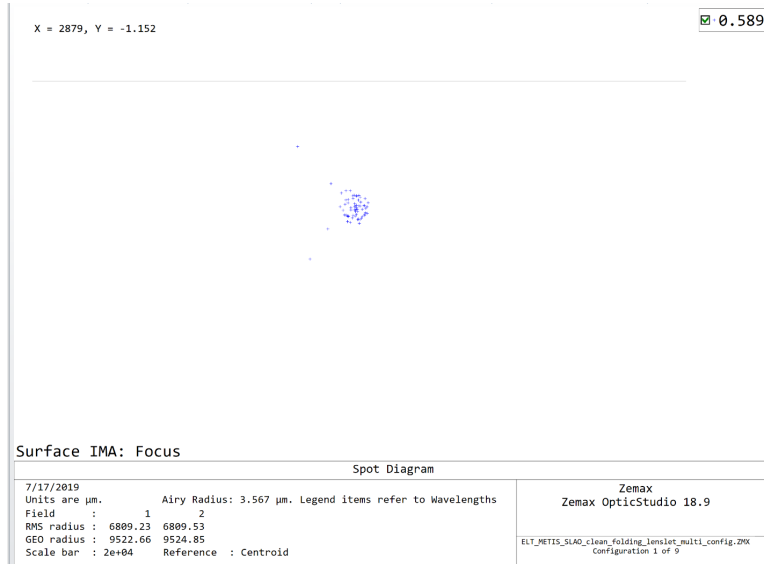


FIGURE 4.2: A Figure with the calculated Airy Disk radius in the data sheet on the bottom left. The coordinates in the top left are displayed in microns. It should be noted that there is some aberration effect taking place.

When the lenslet array is substituted in, the Airy disk now has a radius of $3.567 \mu\text{m}$. While it may not be the most scientific way, the next step is to look at the spot and determine its diameter based off of the coordinate positions of the cursor. When the cursor was moved from the top of the spot to the bottom, the cursor changed

roughly $0.5\mu m$. That is a radius of $0.25\mu m$. This means that the spot size is roughly an order of magnitude smaller than the calculated Airy disk by ZEMAX.

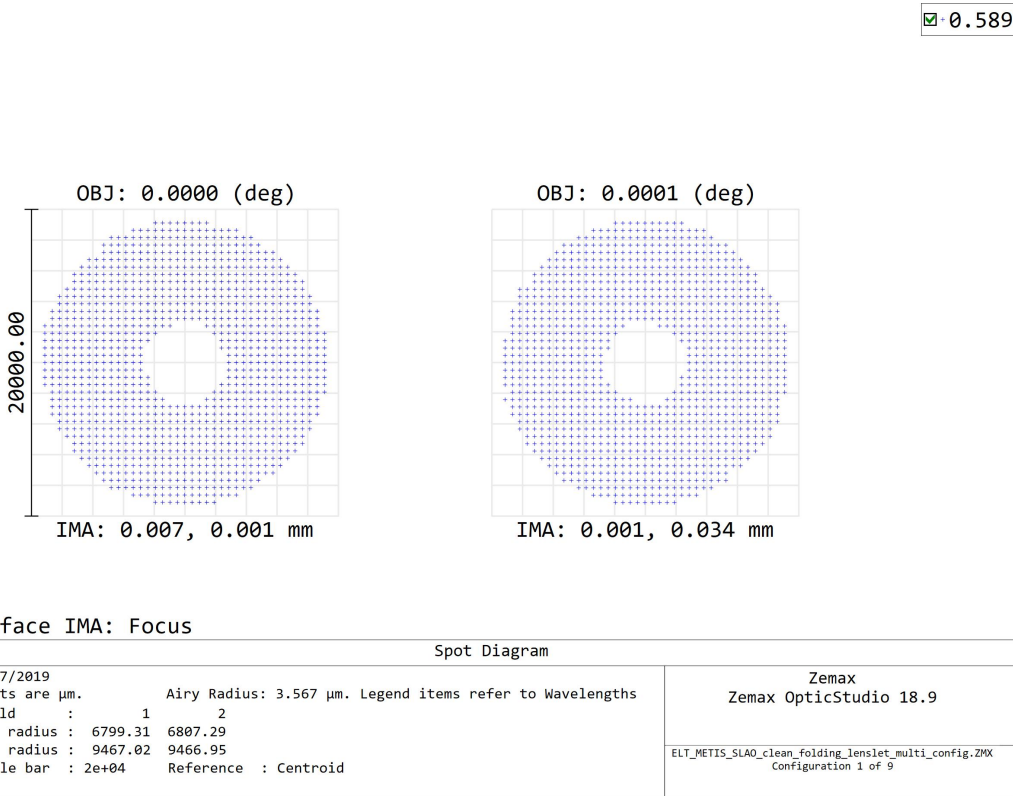


FIGURE 4.3: Here a side by side comparison of two different field angles and their spots. Obviously the spots are too small to see anything revealing.

The full array of spots is 19.6mm across. So side by side comparisons of the fully array do not show anything particularly revealing. However, it does give a good idea what the system will see while in use (Figure 4.3).

4.1.3 Spot Elongation

All of the ELT's lasers are mounted on the perimeter of the telescope support structure. This means that the system will suffer from spot elongation even when pointing at zenith (Figure 4.4). Since the Sodium layer in the Earth's atmosphere has an approximate thickness of 10 km, there will be illumination all along that thickness. We made the assumption that the laser spot would be pointed to directly above the telescope. Therefore, we assumed that the on-axis portion of the laser was in the center of the Sodium Layer. How this was handled in ZEMAX was to find the off-axis angle for the min and max altitude of the spot at each zenith angle. Each of these were a separate configuration in ZEMAX.

From these configurations, it is apparent that there is the greatest amount of spot elongation when pointing at zenith. It should also be noted that Figures 4.5, 4.6, and 4.7, were evaluated with the annular mirror having a central obscuration (Diameter= 42.9mm [3]) in it to simulate the hole in the mirror. There does not appear to be any light lost from the central obscuration from spot elongation.

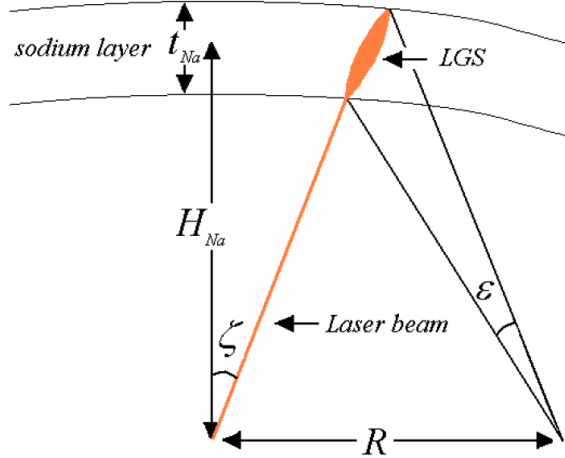


FIGURE 4.4: A figure showing an example of what causes spot elongation [17]

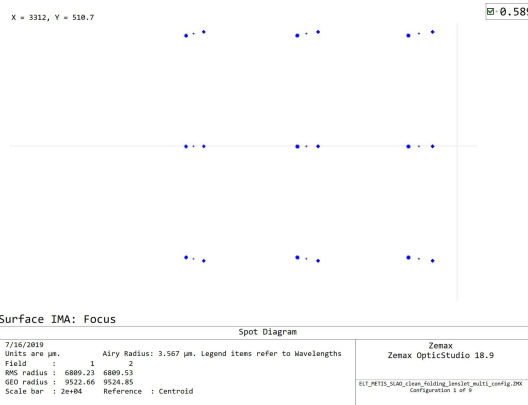


FIGURE 4.5: 80km [14]

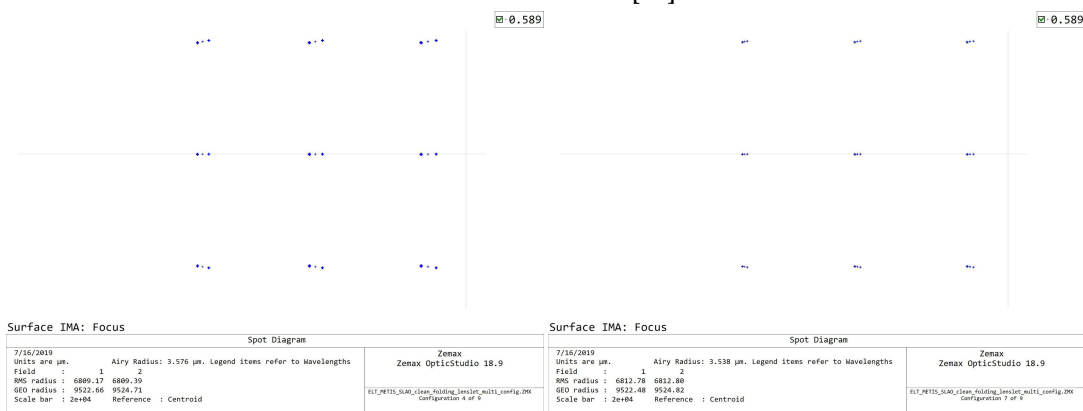


FIGURE 4.6: 105km
[14]

FIGURE 4.7: 160km
[14]

4.2 Wavefront Map

One of the requirements for METIS is to achieve certain Strehl ratios at certain optical bands. In the 2010 SPIE article "Designing the METIS Adaptive Optics System", certain wavefront errors were presented [21]. The goal of the AO system was to achieve

below a 360 nm RMS WFE[21]. Since ZEMAX outputs wavefront map calculations in units of waves, a simple calculation can be made. Since the SLAO system works with only one wavelength (589 nm) all that needs to be done is multiply the wave fraction number.

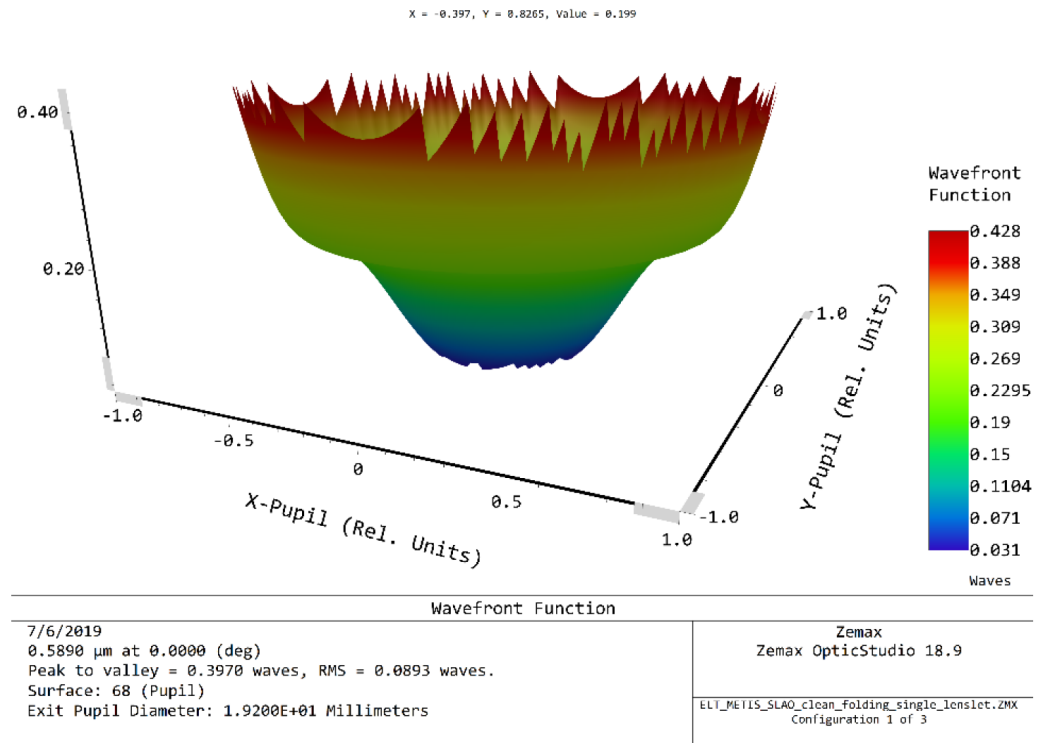


FIGURE 4.8: Here is a map of the wavefront at the lenslet array. PTV = 234 nm ; RMS = 52.6 nm.

In Figure 4.8, we can see that the on axis performance is almost a factor of 7 better than the requirement. This allows room for other errors such as telescope errors, non-common path errors, and other physical errors. For a full list of wavefront characteristics, see Appendix A.

4.3 Aspherical Component

One of the main purposes of this research was to look into ways to minimize aspherical surfaces. However, having one asphere can make a design cheaper in the end. It is important however to have a manufacturable asphere. In general, the more material that needs to be removed, the more expensive the part. The amount of material needed to be removed for this aspherical component is all fractions of a millimeter and over an aperture size of 20 mm. Upon inspection, the map appears close to a parabolic shape. All of these are good factors for manufacturing an aspherical component.

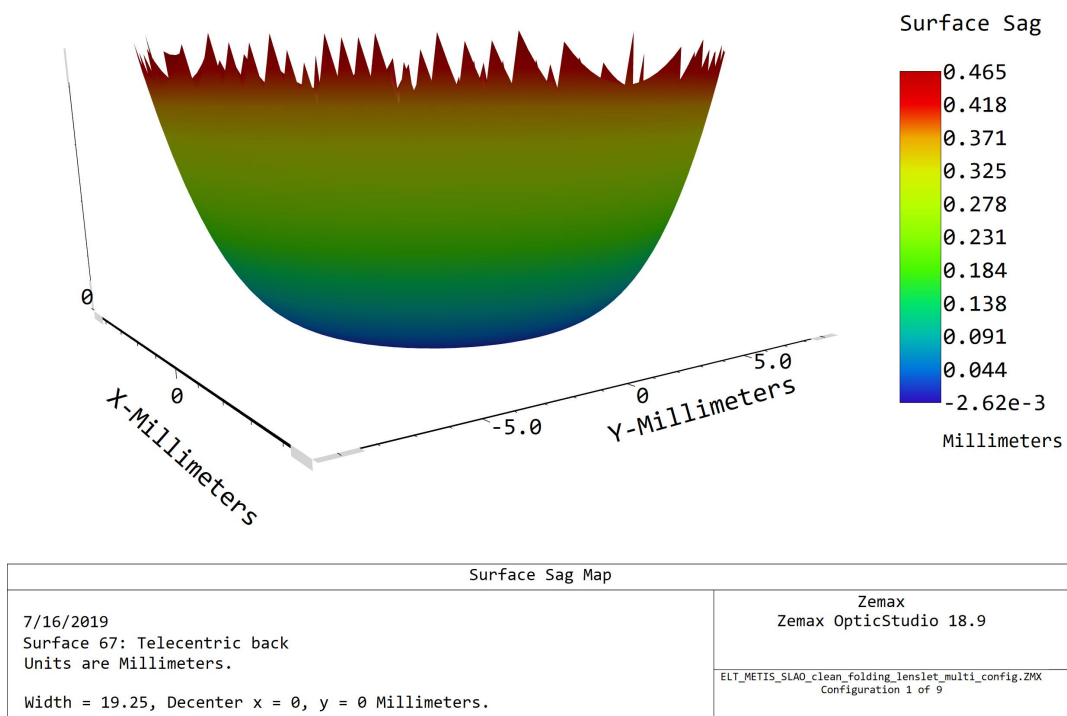


FIGURE 4.9: A Figure showing a surface map of the aspherical component.

Chapter 5

Conclusion

In conclusion, a successful optical design was engineered within the constraints laid out by the restrictions of the METIS group and that of adaptive optics systems. Despite not getting to a point where a new mechanical design was made, there are rough dimensions that the optical design can provide. The optical design has rough physical volume of:

- $L \approx 1.2m$
- $W \approx 400mm$
- $H \approx 900mm$

Of course these dimensions will increase slightly in order to create an opto-mechanical design that can properly support the system. The original design provided by Benjamin showed that a SLAO system could be implemented but showed to be expensive. One of the driving factors in this research was to take a concept of a SLAO system and prove that it could be easily manufactured with the least amount of cost. The design incorporates all but one, spherical surfaces and is made out of the same glass type. The glass type chosen was BK7. BK7 is known as a easily manufacturable material and is not brittle. All lenses are mounted normal to gravity and should have limited long-term wear.

The system has shown to have good performance with spot sizes smaller than the Airy disk as well as wavefront errors less than what was in the requirements. Given more time, the wavefront could be further improved. The WFE, showed that it suffered in piston. Simply put, if the lenslet array was translated a few tenths of a micron, the WFE would be ± 0.2 waves PTV.

Another issue that needed to be solved was to implement a simple solution for the change in laser distance. Similar to the HARMONI AO system, a telescoping fold mirror system was integrated into the design. This prevented the necessity of have a moving camera and glass, making the system less susceptible to failure.

Given more time, there were a few things that could be improved. The system still needs a mechanical design to progress further in its development. However, the components used in the make up of the original optical design can be used in the new design. Both translation stage and cage beams can be used in the mechanical design. It was also noted that some lenses may be too thin. It will be important to go back and change some lenses to be thicker in order to prevent deformations of the optics.

Despite not completing a full opto-mechanical design, the design looks promising with its ease of manufacturing, and total size. It is still unclear if the ESO will accept a SLAO system for METIS. However, the work done by myself and Benjamin Arcier show that a SLAO system does have the performance necessary to perform good science and can be made at a relatively low cost compared to a LTAO system.

Appendix A

Wavefront Maps

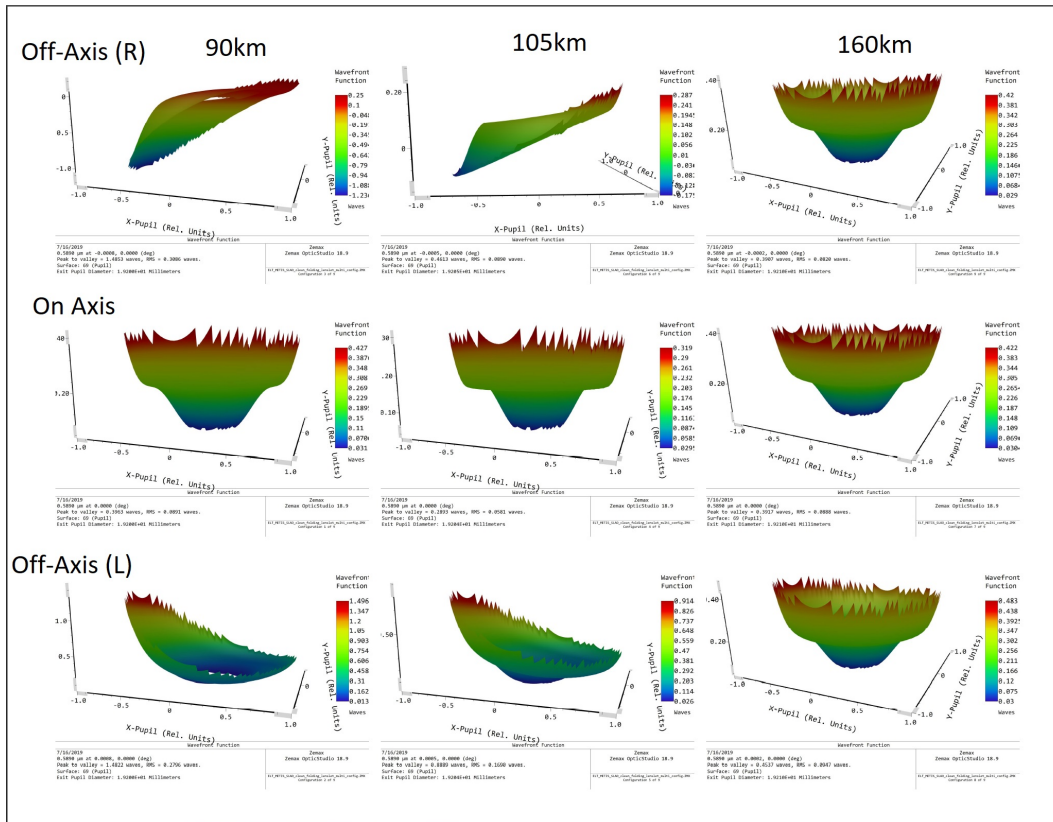


FIGURE A.1: All wavefront maps for on axis and off axis spots at different Zenith angles

Bibliography

- [1] 220 mm Linear Translation Stage, Direct-Drive Servo Motor. URL: https://www.thorlabs.com/newgroupage9.cfm?objectgroup_id=5305.
- [2] AOModes. URL: https://www.eso.org/sci/facilities/develop/ao/ao_modes/.html.
- [3] Benjamin Arcier. "Single Laser Adaptive Optics system for the ELT/METIS: Feasibility and Performance study". Dec. 2018. URL: <http://resolver.tudelft.nl/uuid:f2f4f0b0-0f13-4874-a191-a0ce7102b60a>.
- [4] Naoshi Baba, Syuzo Isobe, Youji Norimoto, and Motokazu Noguchi. "Stellar speckle image reconstruction by the shift-and-add method". In: *Appl. Opt.* 24.10 (May 1985), pp. 1403–1405. DOI: [10.1364/AO.24.001403](https://doi.org/10.1364/AO.24.001403). URL: <http://ao.osa.org/abstract.cfm?URI=ao-24-10-1403>.
- [5] Thomas Bertram et al. "Single conjugate adaptive optics for METIS". In: vol. 10703. 2018. DOI: [10.1117/12.2313325](https://doi.org/10.1117/12.2313325). URL: <https://doi.org/10.1117/12.2313325>.
- [6] B. R. Brandl et al. "Status of the mid-infrared E-ELT imager and spectrograph METIS". In: *Ground-based and Airborne Instrumentation for Astronomy VI*. Vol. 9908. Proceedings of the SPIE. Aug. 2016, p. 990820. DOI: [10.1117/12.2233974](https://doi.org/10.1117/12.2233974).
- [7] Bernhard R. Brandl et al. "Status of the mid-IR ELT imager and spectrograph (METIS)". In: vol. 10702. 2018. DOI: [10.1117/12.2311492](https://doi.org/10.1117/12.2311492). URL: <https://doi.org/10.1117/12.2311492>.
- [8] B.R. Brandl. *Executive Summary*. Version 1-1. 2019.
- [9] Kjetil Dohlen et al. "Opto-mechanical designs for the HARMONI adaptive optics systems". In: vol. 10703. Proceedings of the SPIE. 2018. DOI: [10.1117/12.2313651](https://doi.org/10.1117/12.2313651). URL: <https://doi.org/10.1117/12.2313651>.
- [10] Gert Finger, Ian Baker, Domingo Alvarez, Derek Ives, Leander Megragan, Manfred Meyer, Jörg Stegmeier, and Harald J. Weller. "SAPHIRA detector for infrared wavefront sensing". In: vol. 9148. 2014. DOI: [10.1117/12.2057078](https://doi.org/10.1117/12.2057078). URL: <https://doi.org/10.1117/12.2057078>.
- [11] John E. Greivenkamp. *Field guide to geometrical optics*. SPIE Press, 2004.
- [12] Eugene Hecht. *Optics*. 5th. Pearson, 2017, pp. 183–184.
- [13] Dan Hill. *How to Model a Mixed Sequential/Non-Sequential System*. Dec. 2015. URL: <https://customers.zemax.com/os/resources/learn/knowledgebase/how-to-model-a-mixed-sequential-non-sequential-sys>.
- [14] Patrick Hoge. URL: <http://www.patrickhoge.com/>.
- [15] Christoph Keller. *Foundations of Optics*. July 2019. URL: https://home.strw.leidenuniv.nl/~keller/Teaching/ATI_2018/ATI_2018_L01_FundamentalOptics.pdf.
- [16] Claire Max. *Introduction to AO*. July 2019.

- [17] N. Moussaoui, B. R. Clemesha, R. Holzlöhner, D. M. Simonich, D. Bonaccini Calia, W. Hackenberg, and P. P. Batista. "Statistics of the sodium layer parameters at low geographic latitude and its impact on adaptive-optics sodium laser guide star characteristics". In: *Astronomy and Astrophysics* 511 (2010). DOI: [10.1051/0004-6361/200913281](https://doi.org/10.1051/0004-6361/200913281).
- [18] *Productdetails: item Industrietechnik GmbH*. URL: <https://product.item24.de/en/products/product-catalogue/productdetails/products/construction-profiles-8-1001042794/profile-8-40x40-light-natural-2633/>.
- [19] Vladimir Sacek. 6.5. *Strehl ratio*. URL: <https://www.telescope-optics.net/Strehl.htm>.
- [20] Iuliia Shatokhina, Andreas Obereder, Matthias Rosensteiner, and Ronny Ramlau. "Preprocessed cumulative reconstructor with domain decomposition: a fast wavefront reconstruction method for pyramid wavefront sensor". In: *Appl. Opt.* 52.12 (Apr. 2013), pp. 2640–2652. DOI: [10.1364/AO.52.002640](https://doi.org/10.1364/AO.52.002640). URL: <http://ao.osa.org/abstract.cfm?URI=ao-52-12-2640>.
- [21] R. Stuik et al. *Designing the METIS adaptive optics system*. 2012. DOI: [10.1117/12.926137](https://doi.org/10.1117/12.926137). URL: <https://doi.org/10.1117/12.926137>.
- [22] Laird A. Thompson, Scott W. Teare, Samuel L. Crawford, and Robert W. Leach. "Rayleigh Laser Guide Star Systems: UnISIS Bow-Tie Shutter and CCD39 Wavefront Camera". In: *Publications of the Astronomical Society of the Pacific* 114.800 (2002), pp. 1143–1149. DOI: [10.1086/342764](https://doi.org/10.1086/342764). URL: <https://arxiv.org/abs/astro-ph/0207074v1>.